NASA/USRA
Advanced Design Program

The Ohio State University

OSU Team 2

Hypersonic Test Vehicle Design

OSU II Design Team
Conceptual Hypersonic Flight Vehicle Design

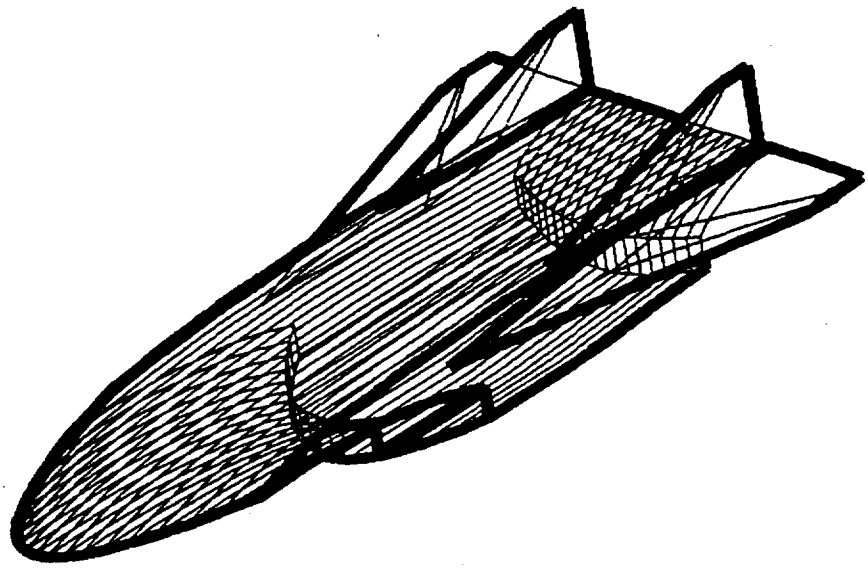

Cameron Cunningham
Larry Kucaric
Eric Polstra
Ron Ratell
Greg Stanislaw

Professor: Dr. Gregorek
T.A.: Duane Detwiler

Abstract

This report analyzes and presents a preliminary design for an experimental hypersonic vehicle. This plane will have a cruise speed of Mach 12 for one minute at an altitude of 120,000 feet. The major design areas of aerodynamics, propulsion, and weights are discussed in depth. An elementary analysis of thermal protection, trajectory and cost is also presented. Finally, a discussion of future plans and recommendations is given, and overall conclusions are drawn.

Table of Contents

List of Figures

List of Tables

1. Introduction

Modern technology is reshaping our world at a staggering rate. Communication and defense have become reliant on man-made satellites for data relay and acquisition. The maintainance and retrieval of these high-tech systems is necessary to keep operations on line and running at peak economic efficiency. The development of a single-stage-to-orbit vehicle would provide an inexpensive means of achieving these goals. At a mission cost of approximately 1/10 of the space shuttle, the NASA proposed X-30 would use modern airbreathing propulsion systems to reach low Earth orbit, perform a specific function while in orbit, and land conventionally.

This report desribes an experimental hypersonic test bed for such an aircraft. The test vehicle will examine the performance of the scramjet engine under true flight conditions, along with other hypersonic characteristics. Eventually, these experiments will lead to the development of the X-30 or a similiar vehicle. The design requirements for this project were set as shown in the following table.

Test Speed	**Mach 12-15**
Test Time	**1 Minute at Steady Conditions**
Test Altitude	**100,000 - 120,000 feet**
Propulsion	**Airbreathing**
Payload Weight	**1000 lbs**
Payload Volume	**35 cubic feet**
Operational Costs	**2 - 3 billion dollars**

Table 1: Design Requirements

2. Summary

The hypersonic vehicle proposed was optimized for a one minute cruise at a speed of Mach 12 while at an altitude of 120,000 ft. The vehicle will be unmanned and missile launched from the ground. One of the main objectives of the project lies in the testing of the scramjet engine system. Therefore, a lifting body design was chosen, with the entire underbody defined to accomodate top scramjet performance. Figure 1 provides a three view of the proposed plane. The diffuser at the bow not only compresses the airflow via an oblique shock, but also acts as a lifting surface. The rear nozzle was designed to expand the engine exhaust gas to atmospheric conditions.

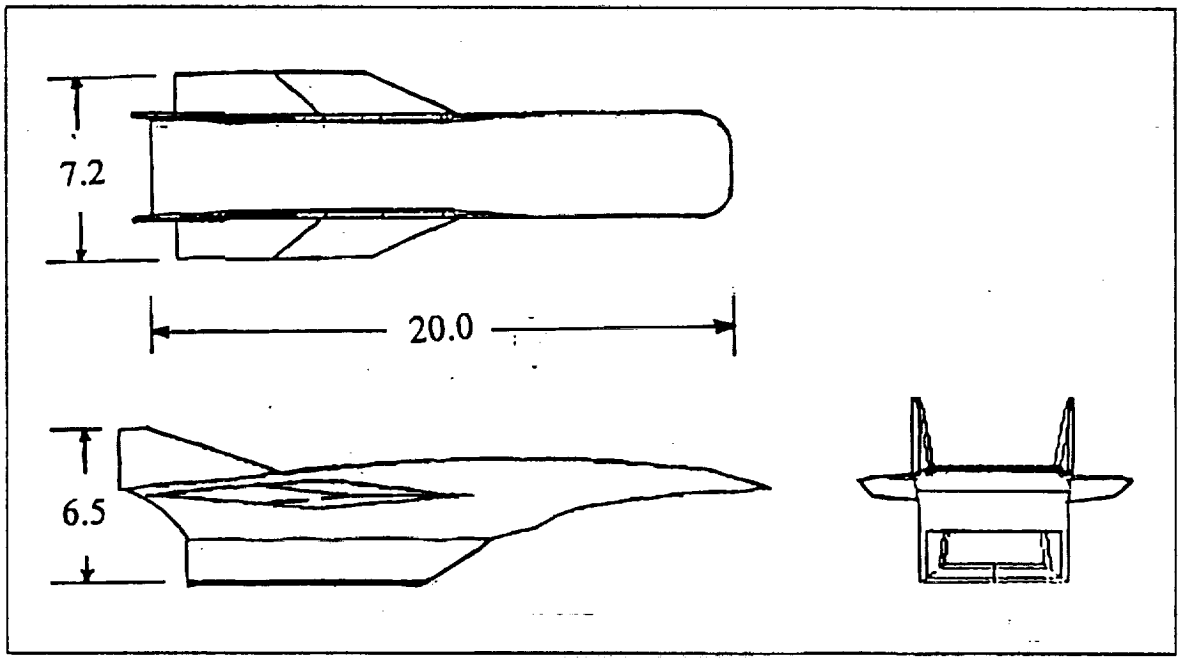

Figure 1: 3-View of Design

Booster rockets will power the vehicle to the test conditions. To keep costs to a minimum, current military and space missiles were investigated. As a result, one two-stage Minuteman missile with solid propellant were chosen. Once at the test conditions, the boosters are dropped, and one scramjet engine maintain the cruise speed for one minute. This engine will use liquid hydrogen as its fuel.

The weight analysis of our vehicle was performed using a component build-up method, the Wright-Patterson code PDWAP, and segments of the HASA program. Most of the vehicle's weight is comprised of propulsion and structures, which work together to develop the thrust necessary to maintain the high cruise speed. The planform incorporates mutiple fuel tanks to allow for cylindrical design and fuel sequencing. This will allow center of gravity control and ease of maintanence.

Due to the high surface temperatures on the leading edges and around the engines, an active thermal protection system is incorporated. Liquid hydrogen will be channeled from storage tanks to the hot spots, and then to the scramjet engines. Furthermore, a passive cooling system will embody the entire aircraft.

The vehicle/booster rocket system is designed to be launched from a coastal region for safety reasons. A simple representation of the vehicle with its booster is shown in Figure 2. The entire system will be given a slight angular momentum at launch, creating level flight when the second stage is jettisoned at the test altitude. Upon completion of the one minute test, the vehicle will coast to subsonic speed, and deploy drag and landing parachutes. Splashdown will occur approximately 800 miles from takeoff. A list of specifications is given in Table 2.

Length	20.0 feet
Width	7.2 feet
Height	6.5 feet
Wing Sweep	75.5 degrees
Takeoff:	
Distance to cruise	170 miles
Weight (with missiles)	76,300 lbs
Cruise:	
Mach Number	12.0
Altitude	120,000 feet
Distance	140 miles
Landing:	
Distance	500 miles
Weight	6,700 lbs
Engines	1 scramjet
Mission Time	10 minutes

Table 2: Test Vehicle Specifications

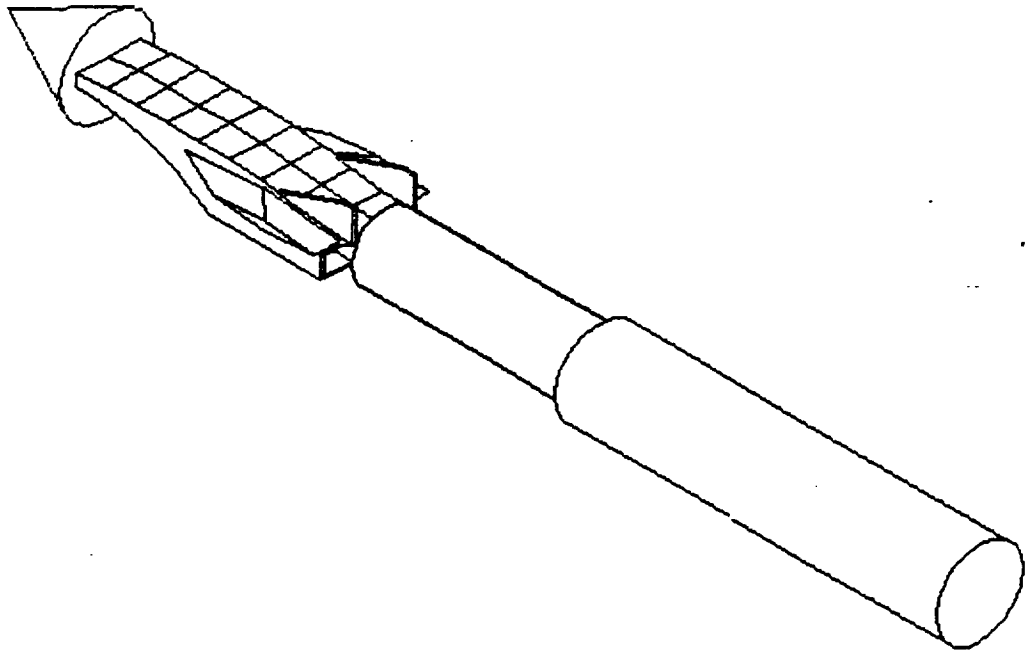

Figure 2: Rocket and Booster

3. Aerodynamics

The following sections will give a brief overview on the decision to use our configuration, describe the methods used to determine the aerodynamic properties of the aircraft through the subsonic, transonic, supersonic, and hypersonic regimes in which it travels, and finally discuss the results of our analysis.

The aircraft we have designed to meet the mission specifications is a lifting body. We feel this would be the best configuration to test a scramjet engine at the required Mach number and altitude. The key advantages to using the lifting body are high volumetric efficiency, better TPS weight, and better aerodynamic efficiency at high altitudes and Mach numbers due to external diffusion. The underside of the forefront of the fuselage is used to diffuse the flow into the inlet of the engines. The flow must be slowed from the free-stream Mach number (M_∞) of 12 to Mach 6 at the inlet. This was accomplished utilizing the method of characteristics. Applying oblique shock relations on the resulting diffuser confirmed that the required inlet Mach number was achieved. The wings of the aircraft have a 75° sweep angle, and the aircraft's span is 7.2 feet. We are employing a symmetrical diamond-wedge airfoil with a half-angle of 5°, an aspect ratio of 0.745, and a thickness-to-chord ratio of 0.0875.

As work progressed on designing the most capable aircraft to meet the mission requirements, the aircraft changed in size and weight. In order for the aircraft to reach Mach 12 at 120,000 feet using the rockets proposed by the propulsion team, the aerodynamic team needed to downsize the vehicle. The limiting factor is the average acceleration of 200 ft/s^2 needed to reach the desired altitude and velocity. To accomplish this we cut down the amount of drag on the entire system (rocket and aircraft), as well as minimized the weight.

Subsonics/Transonics:

The most current version of the hypersonic vehicle has the aircraft being boosted to near test conditions, then running the scramjets for the required test time, and finishing the flight with a gliding descent to an altitude ideally suited for parachute deployment and recovery. In regards to this mission profile, transonic and subsonic analysis will need to be performed for the aircraft's gliding characteristics down to an altitude suitable for parachute deployment.

The two most accurate methods available to us for subsonic analysis is APAS and to actually build and wind tunnel test a scale model of the vehicle. Time constraints have delayed these types of analysis until the future. The analysis that was completed was accomplished by comparing published data of similarly shaped lifting bodies.

Subsonic analysis of aircraft with aspect ratios, AR, greater than 3 have aerodynamic coefficients that behave linearly with change in angle of attack. But, the lift curve slopes for planforms with AR less than 3 behave in a nonlinear fashion. The linear theories underestimate the lift for low AR planforms due to completely different flow patterns around slender bodies and swept wings. The characteristic flows past these shapes feature strong cross flows which lead to separation of flow at highly swept, wing leading edges and body sides. These flows, if created by sharp leading edges, can develop into powerful vortices which force higher energy air from outside of the boundary layer into the top surface preceding the vortex generator thus delaying flow separation.

In order to estimate parachute deployment velocities, the aircraft stall speed is approximated conservatively by using; a thin airfoil α max of 15 degrees (.2618 radians), $dCl/d\alpha$ of 0.108 per degree (6.188 per radian), Sw of 95 square feet, density altitude at 10,000 feet of 0.001756 slug/cubic ft, C1 non-linear lift factor of 2.5, gliding weight of 6500 lbs, and the following lift coefficient equation:

$$CL = (dCl/d\alpha)*\alpha + C1*\alpha*\alpha$$

This equation gives a CLmax of 1.79 and allows for solving the aircraft's stall speed.

Vstall = 210 feet per second (143.18 mph).

The following is a table of significant aerodynamic configuration parameters:

b	7.2 feet
C_{tip}	1.92 feet
λ	0.16457
Croot	11.7 feet
Cmac	10.3 feet
AR Wing	1.6977
AR Body	0.950
Leading Edge Seep Angle	80 degrees
Maximum Thickness Sweep Angle	66.3 degrees
S_{wing}	95.425 ft^2
C.G. Location from nose	12.7 feet
t/c ratio (5 degree half angle)	5.0 %

Table 3: Wing Data

To add to the complication of subsonic analysis, the lift and drag characteristics of a wing and body do not add directly, due to a wing-body interference factor. The zero lift drag coefficients for various Mach numbers greater than 2 were determined from the group's computer code. To obtain zero lift

drag coefficients for various Mach numbers in the transonic and subsonic region, a careful comparison to published Cdo vs M data gives:

Cdo	Mach Number
0.042	0.30
0.055	0.70
0.105	1.00
0.095	1.20

Table 4: Comparison of Subsonic/Transonic Cdo

Supersonic/Hypersonic Theory

The aerodynamic analysis of our aircraft design in the supersonic and hypersonic regime was accomplished mainly using Prandtl-Meyer Shock-Expansion Theory (Anderson 100). Since this theory is inviscid, skin friction needed to be added. The skin friction was modeled using incompressible flate plate turbulent skin friction and correcting for compressibility effects (Nicolai 2-25). The Method of Characteristics was also used in designing the underside of the aircraft for supersonic diffusion. Note that the Prandtl-Meyer Shock-Expansion Theory and the Method of Characteristics are for two-dimensional, steady flow. The following is an overview:

Prandtl-Meyer Shock-Expansion: This theory was developed from purely geometrical considerations of oblique shock and expansion waves. When a supersonic flow encounters a compression corner, the disturbance is not able to propagate upstream due to the flow's supersonic speed. Therefore a shock must form in order to divert the flow parallel to the compression surface. In looking at an oblique shock wave in Figure 3,

we see there are components of the freestream ahead of the oblique shock perpendicular and parallel to the oblique shock.

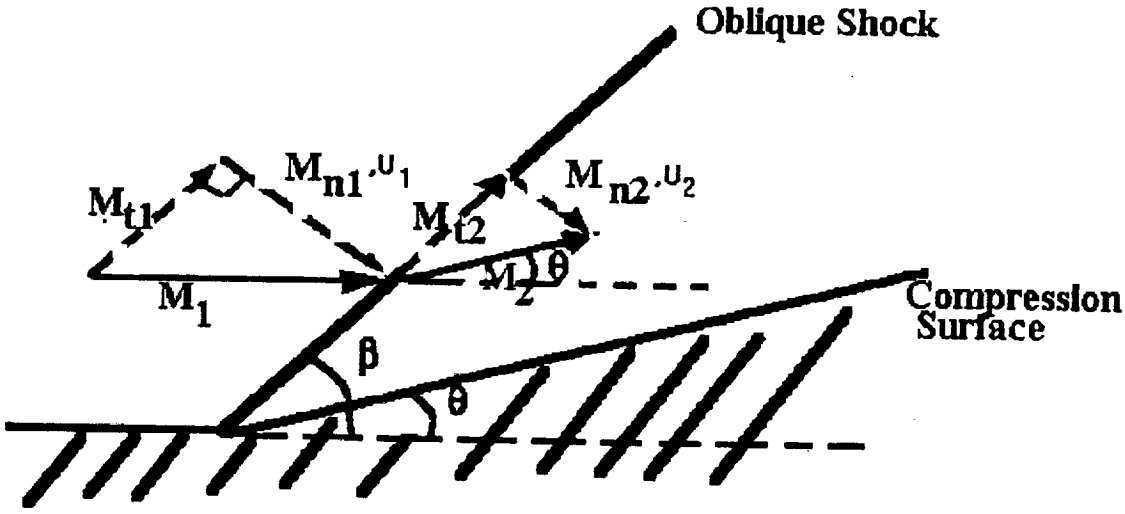

Figure 3: Oblique Shock

Writing these components in terms of the freestream mach number and the oblique shock we have:

$$M_{t1}=M_f\sin(\beta-\theta) \quad (1)$$

$$M_{n1}=M_f\sin(\beta) \quad (2)$$

where M_{t1}= tangetial mach number

M_{n1}= normal component of mach number

β= oblique shock angle

θ= compression corner angle

Using the integral form of the conservation equation (Anderson 36) in two components, one tangential and one perpendicular to the oblique shock, one finds that the tangential component of the flow field is conserved across the oblique shock wave. For the normal component of the freestream relative to the oblique shock wave, it can be shown that the normal shock relations obtained from normal shock continuity, momentum and energy equations can be used, yielding:

$$\rho 2/\rho 1=(\gamma+1)M_{n1}{}^2/((\gamma-1)M_{n1}{}^2+2) \tag{3}$$

$$p2/p1=1+(2\gamma/(\gamma+1))(M_{n1}{}^2-1) \tag{4}$$

$$M_{n2}{}^2=(M_{n1}{}^2+(2\gamma/(\gamma-1))/((2\gamma/(\gamma-1))M_{n1}{}^2-1) \tag{5}$$

where M_{n2}= normal mach number after oblique shock

p2= static pressure behind oblique shock

$\rho 2$= density behind oblique shock

$\rho 1$= freestream density

p1= freestream pressure

M_{n1}= normal component of freestream mach number

Integrating the continuity equation across an oblique shock wave yields:

$$\rho 1u1=\rho 2u2 \tag{6}$$

From the geometry in Figure 3, we have the relation:

$$\frac{\tan(\beta-\theta)}{\tan(\beta)}=\frac{u_2}{u_1} \tag{7}$$

Combining equations (6),(1),(3) and (7) we obtain:

$$\tan(\theta)=2\cot(\beta)[(M_1^2\sin2(\beta)-1)/(M_1^2(\gamma+\cos(2\beta)+2))] \quad (8)$$

This relationship is the fundamental relationship between θ, β and M_1. From this relation, given any of the two variables, the third can be determined. Graphs of this function are often used, but were insufficient for our analysis. Therefore, a numerical technique needed to be employed. In our anlaysis, the freestream conditions and the compression surface angle were known and the oblique shock angle was the unknown.

The normal mach number, M_{n1}, is determined once the oblique shock angle, β, is known. From this, using equations (2), (3), (4) and (5), the conditions behind the shock are easily calculated. Note that from equation (5), there can exist two values of β which will satisfy the relationship. These values correspond to strong and weak shock solutions of the oblique shock wave. The strong solution results in the flow being entirely subsonic behind the oblique shock, while the weak corresponds to the flow being supersonic behind the shock. This is a result of the magnitude of the back pressure behind the shock. Our analysis assumed only weak shock solutions over the entire body of the aircraft.

Expansion waves are a result of supersonic flow being turned away from itself as shown in Figure 4.

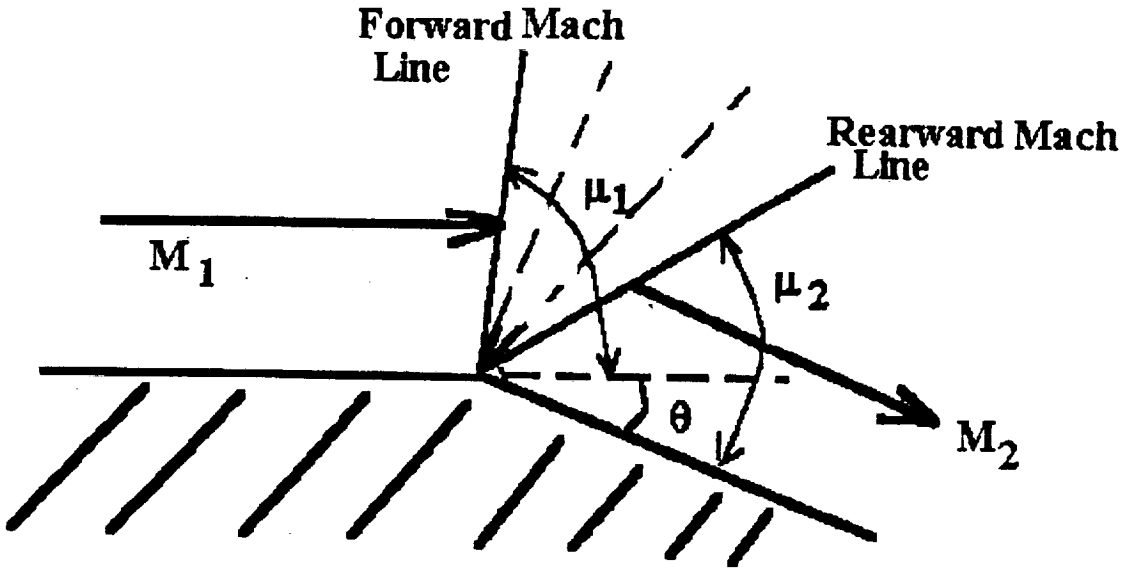

Figure 4: Supersonic Expansion Wave

Shown in Figure 4 are the forward and rearward mach lines with two intermediate mach lines. In reality, there is an infinite number of mach lines between these two lines and the collection of all these lines make up the expansion fan. In Figure 4, μ is the mach angle for the given conditions at each interval. Without going into detail on the derivation of the Prandtl-Meyer function for supersonic expansion waves, the result, which can be found in any text on supersonic flow, will be stated (Anderson 134):

$$\nu(M)=\sqrt{\frac{\gamma+1}{\gamma-1}}\tan^{-1}\sqrt{\frac{\gamma+1}{\gamma-1}(M^2-1)}-\tan^{-1}\sqrt{M^2-1} \qquad (9)$$

The relationship between the Prandtl-Meyer function and the expansion angle θ is given by:

$$\theta = \nu(M_2) - \nu(M_1) \tag{10}$$

Therefore, given the expansion angle, θ, and the initial flow mach number, M_1, the Prandtl-Meyer function for the mach number after the expansion can be determined from equation (10). Tabulated results for the Prandtl-Meyer function for air are widely available, but this was not practical for our needs. Again, an iteration technique was needed to solve for the mach number given the value of the Prandtl-Meyer function. This will be discussed in the section entitled Fortran Code.

Skin Friction: The skin friction for our design was modeled using incompressible flat plate skin friction for a turbulent boundary layer modified with a correction factor for compressibility effects. The skin friction coefficient, C_{fi}, for incompressible flow is given by (Nicolai 2-25):

$$C_{fi} = \frac{.074}{R_e^{0.2}} \tag{11}$$

where R_e = Reynolds #

Modified for compressibility yields (Nicolai 2-26):

$$C_f = \frac{C_{fi}}{(1+.144M_\infty^2)^{.65}} \tag{12}$$

where M = mach number

The use of equations (11) and (12) might appear invalid for the entire aircraft. Although, if the aircraft was divided into a finite number of panels, then equations (11) and (12) could be used on each panel. This was our approach.

Method of Characteristics: The method of characteristics is a powerful tool in analyzing supersonic, steady, irrotational flow. This method employs solving the partial differential equations for the two-dimensional flow using a characteristic transformation . We will not go into detail here, but will simply state the helpful results that can be used.

A characteristic line in a supersonic flowfield carries with it a constant value. Two characteristic lines intersect at a given point in the flowfield, completely identifying the flowfield at that point. These characteristics are known as K_+ and K_- and have the values of (Anderson 320):

$$K_+ = \theta + \nu(M) \tag{13}$$

$$K_- = \theta - \nu(M) \tag{14}$$

where θ = relative flow angle

ν = Prandtl-Meyer function

Knowing the value of a characteristic of the freestream, we are then able to determine the flowfield at a boundary either given the mach number or the relative inclination of the flowfield at the boundary. Equations (13) and (14) can be added to obtain:

$$\theta = \frac{1}{2}(K_- - K_+) \tag{15}$$

Adding equations (13) and (14) yield:

$$\nu(M) = \frac{1}{2}(K_+ + K_-) \tag{16}$$

Since K_+ at the boundary is also the freestream characteristic, we can arbitrarily assign q for this characteristic to be equal to zero. Therefore, the K_+ is equivalent to the Prandtl-Meyer function for the freestream mach number. Now we can either specify the flow inclination at the boundary and obtain the mach number or we can specify the mach number at the boundary and obtain the flow inclination. The method of characteristics now becomes a powerful tool when designing an external supersonic diffuser. For instance, if a specified mach number is desired at the diffuser exit, then the inclination of the surface at the exit can be determined by solving equation (16) for K_- and substituting this back into equation (15) to obtain:

$$\theta = \nu(M_s) - \nu(M_\infty) \tag{17}$$

where $\nu(M_\infty)$ = Prandtl-Meyer function of freestream

$\nu(M_s)$ = Prandtl-Meyer function at boundary

Now, working backwards from the exit at equal intervals and increasing the mach number to freestream conditions will give you the inclination at each interval of the diffuser. This was used to design the underside of our aircraft.

Having the underside of the test vehicle now defined (external compression surface) the properties can now be determined. The underside forebody was approximated by using 8 panels. Utilizing a FORTRAN code which calculates the properties behind an oblique shock given the properties just before the shock and the deflection angle, the conditions at the inlet to the engine can be determined. Since the method of characteristics gives the contour, the deflection angles of the 8 panels can be calculated relative to the panes before it. In the calculations, the 8^{th} panel is the inlet to the scramjet, so the conditions on the 8^{th} panel are the conditions at the beginning of the inlet. The flow must then be straightened before combustion occurrs. The angle to which the flow must be

straighteded is 19.7° (see Figure 5). The last panel creates an oblique shock which converges on the engine lip when on design at a free stream Mach # of 12 (see Figure 6).

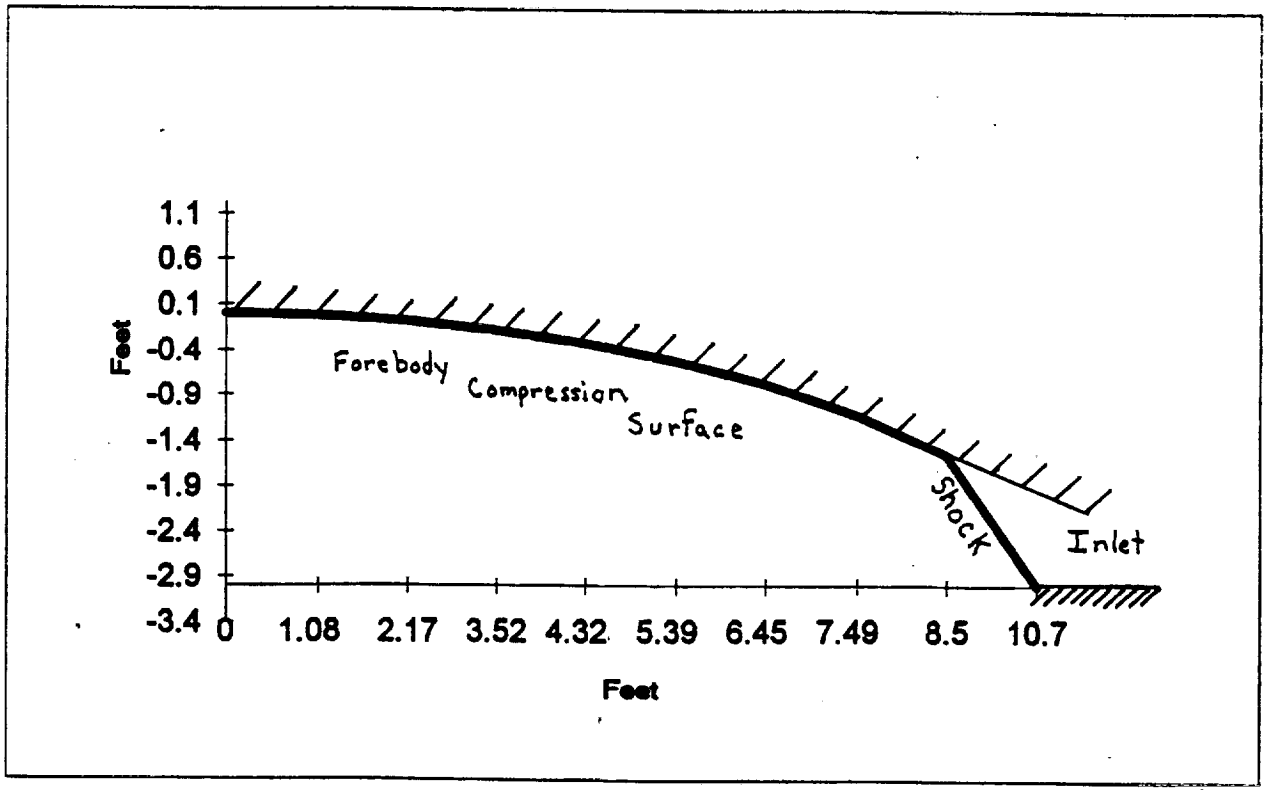

Figure 5: Forebody and Inlet Schematic

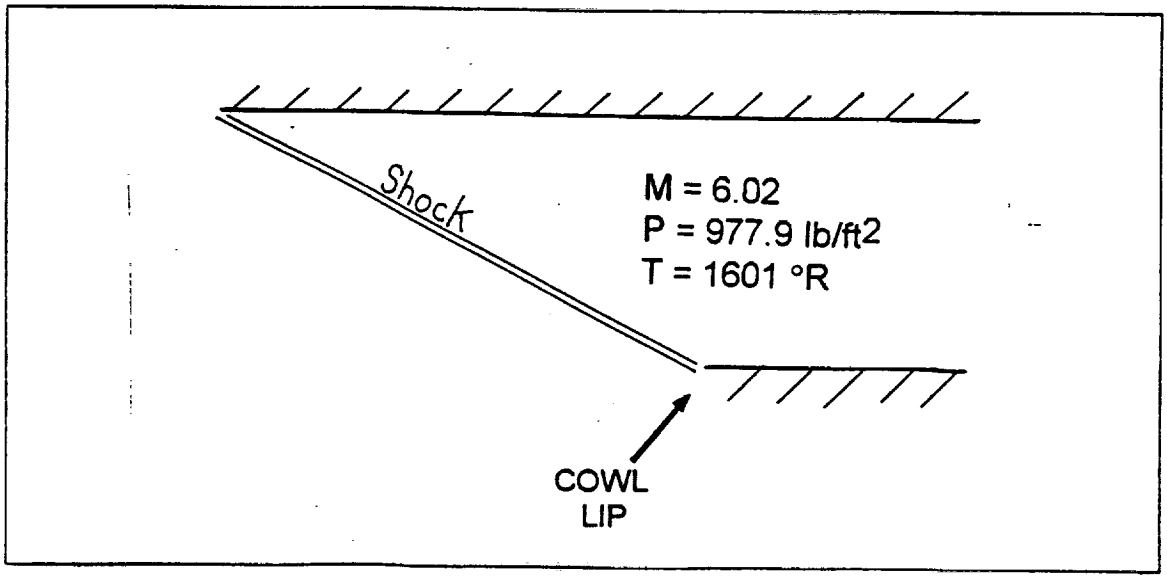

Figure 6: Inlet

Fortran Code

Fortran programs were written to perform the necessary computations to facilitate in calculating the aerodynamic characteristics of our design. Not much detail will be spent on the actual programming, but rather on the numerical techniques used to solve equation (8) for β given M and θ, and the Prandtl-Meyer function, equation (9) for M given the functions value. Also, we will look at how the geometry of the aircraft was specified.

Numerical Techniques: For our purposes, a Newtonian iteration scheme was sufficient. Given a function $F(\beta)=0$, we can solve for β with the following iteration scheme:

$$\beta_{n+1} = \beta_n - \frac{F(\beta)}{F'(\beta)} \tag{18}$$

In equation (18), n denotes the iteration step. As long as the function behaves nicely in the domain where you are iterating, then this technique works rather well. What is meant by behaving nicely is that the derivative is no where zero in the domain and that its sign does not change.

In the case of equation (8), the function $F(\beta)$ is simply:

$$F(\beta) = \tan(\theta) - 2\cot(\beta)\left[\frac{M_1^2 \sin^2\beta - 1}{M_1^2(\gamma + \cos(2\beta)) + 2)}\right] \tag{19}$$

For the strong or weak shock solution the initial guess for β in the iteration should be small for the weak solution (@ 1 degree) and high (@ 89 degrees) for the strong solution.

Solving for M in the Prandtl-Meyer function we have for the function F(M):

$$F(M) = \nu(M) - \sqrt{\frac{\gamma+1}{\gamma-1}}\tan^{-1}\sqrt{\frac{\gamma+1}{\gamma-1}(M^2-1)} + \tan^{-1}\sqrt{M^2-1} \qquad (20)$$

Geometry: The next step was to create the geometry of the aircraft. Since we are only using two-dimensional theory, the aircraft was broken into a number of cross sections. Each cross section consisted of a number of nodes and line elements each having a specified width. Shown in Figure 7 is a typical cross section of a wing used in our analysis. Since we were using two-dimensional theory, each cross section was two-dimensional. To simulate a varying cross sectional wing, a very small width had to be specified in order to approximate the wing.

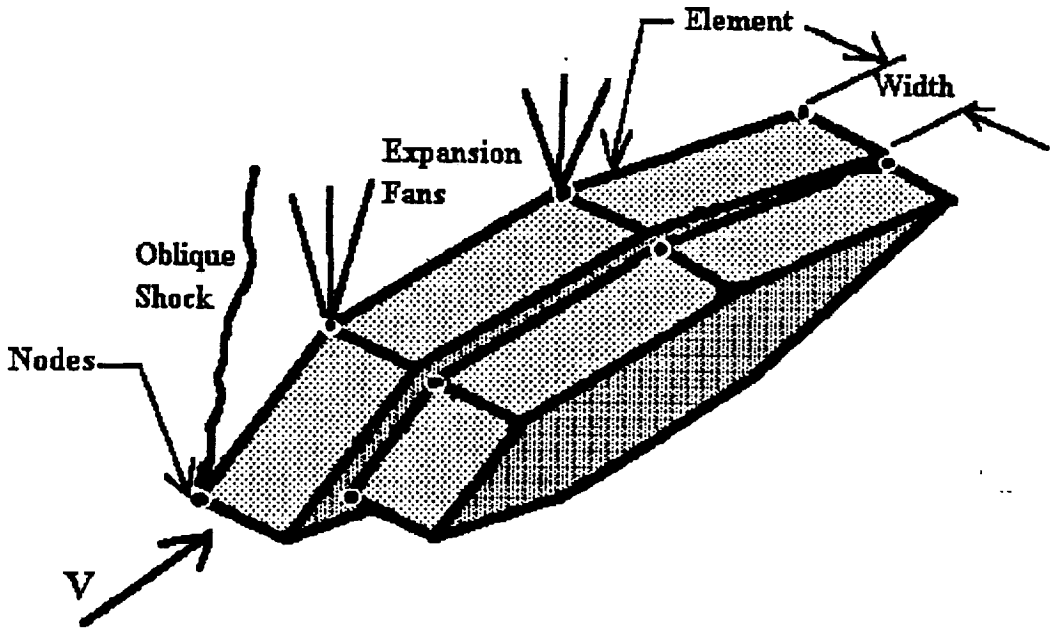

Figure 7: Two-Dimensional Cross Sections

Oblique shocks or expansion waves were then determined by the angle of each panel relative to the freestream velocity vector V. If two panels had coincident nodes, then the flow field conditions from the previous panel would be used to determine the conditions on the following panel.

Aerodynamic Characteristics: It was a simple matter to determine the aerodynamic characteristics of the entire geometric model knowing the flow conditions above each panel, most importantly the pressure and temperature . If the unit normal vector and the area of each panel is known, then the pressure force on each panel is simply the pressure multiplied by the area and its direction is along the negative of the unit normal vector of the panel. The skin friction force for each panel could be obtained by finding the skin friction coefficient for the conditions of each panel [equation (12)] and multiplying this by the area and dynamic pressure. The skin friction force acts parallel along the vector connecting the nodes of each section. Therefore, the total force is simply the sum of the pressure force vectors and the skin friction force vectors.

The dynamic characteristics could also be easily determined by assuming the force vector (skin friction + pressure) acts through the center of each panel. Then, if the center of gravity of the whole model is known, the moments about the center of gravity (c.g.) can be determined by:

$$\vec{M} = \vec{r} \times \vec{F} \qquad (21)$$

Only half of the aircraft configuration was modeled to save computational time. Since the aircraft was symmetric, the results could be doubled.

Verification Example: To verify that that the Fortran program was working correctly, an example of a symmetric wedge airfoil with a 5 degree semi-vertex angle was run through the code at a speed of Mach 3 at sea level and compared with a hand

caluculation. The viscous effects were suppressed in the code so the comparison could be made with the inviscid hand calculation. The following results were obtained:

	Code	Hand Calculation	% Discrepancy
Lift (lb)	0	0	0
Drag (lb)	1451.734	1413.136	2.659

Table 5: Verification of Fortran Code

As you can see, the percentage discrepancy between the two is rather small. The reason for this discrepancy is most likely due to the interpolation from tables and the graphs for the hand calculation. The code on the other hand uses the exact equations. We were pleased with our results.

Results

After running the computer analysis on the aircraft, we found our results to be quite encouraging. The amount of lift generated by the aircraft at cruise conditions is approximately 7500 pounds at 1.5° angle of attack, and the amount of drag is approximately 4900 pounds. This produces an L/D of 1.5 that can be seen in Figure 10. Figure 8 shows the drag polar for the aircraft at cruise (120,000 ft and M_∞=12).

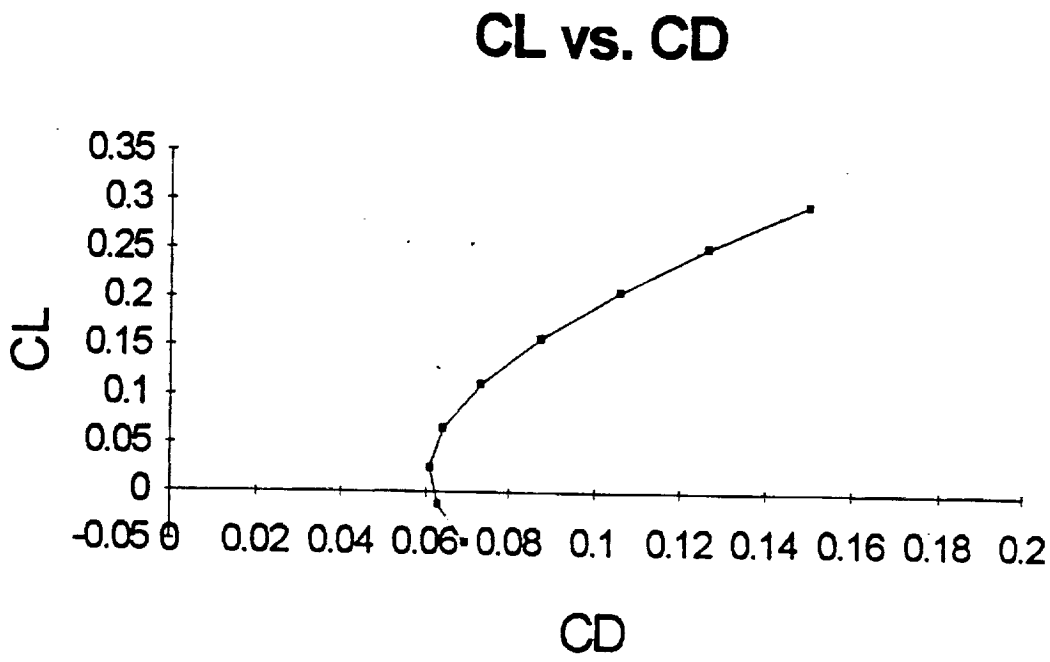

Figure 8: C_L vs. C_D at Cruise

Figure 8 shows that C_{Do} at Mach 12 is approximately 0.061. This is in agreement with the results shown in Figure 9 which plots C_{Do} vs. Mach number.

The rise in C_{Do} begins in the transonic region and is due to adverse pressure gradients. The maximum value of C_{Do} occurs at the sound barrior.

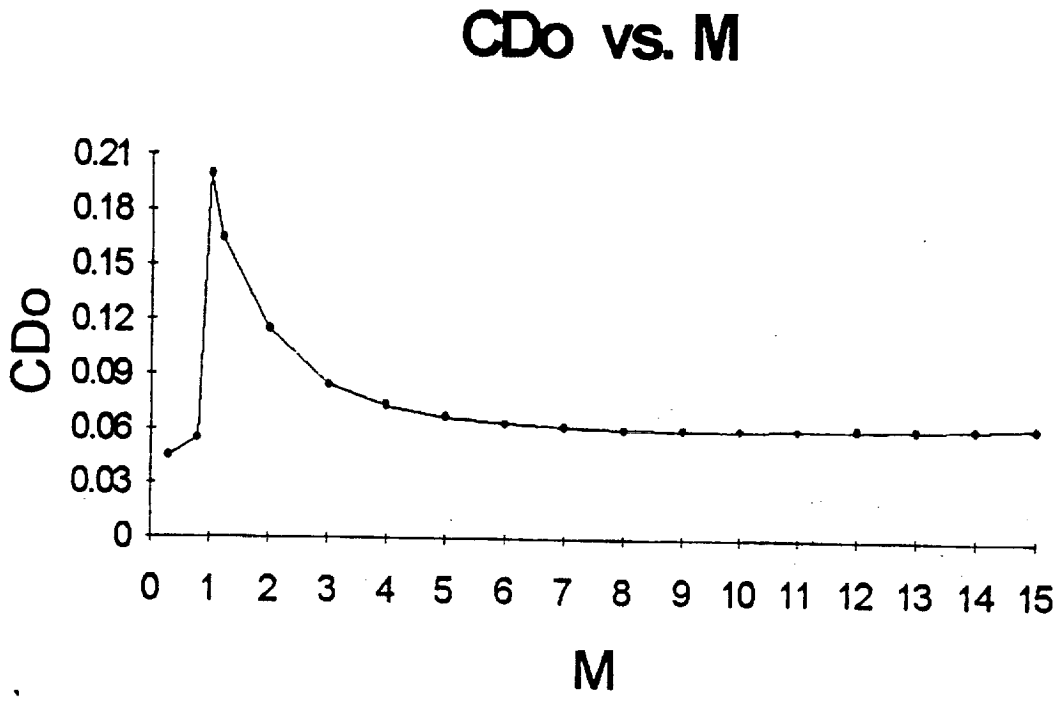

Figure 9: C_{Do} vs. Mach number

For this aircraft it can be seen from Figure 9 that C_{Do}max is approximately 0.19, and it occurs at Mach 1.0. It occurs at this region due to separated flow caused by the adverse pressure gradients which exist because of the shock-boundary layer interaction. After reaching its maximum value, C_{Do} continues to decrease as Mach number increases. This is due to the fact that skin friction drag decreases as M_∞ increases since the shock angle, β , approaches the deflection angle, θ. The plot in Figure 9 compares closely to published wind tunnel results on a similar configuration.

A plot of L/D vs. Mach number is shown in Figure 10. As is expected for a lifting body, the L/Ds are low. The values for our aircraft are slightly lower than published L/Ds which are between 2 and 3.5 for similar lifting body configurations. This is a due in part to our modeling of skin friction drag. The assumption was made that a turbulent boundary

layer existed across the entire body, but in actuality this is not the case. Also, the lift and drag values are based on a two-dimensional wedge.

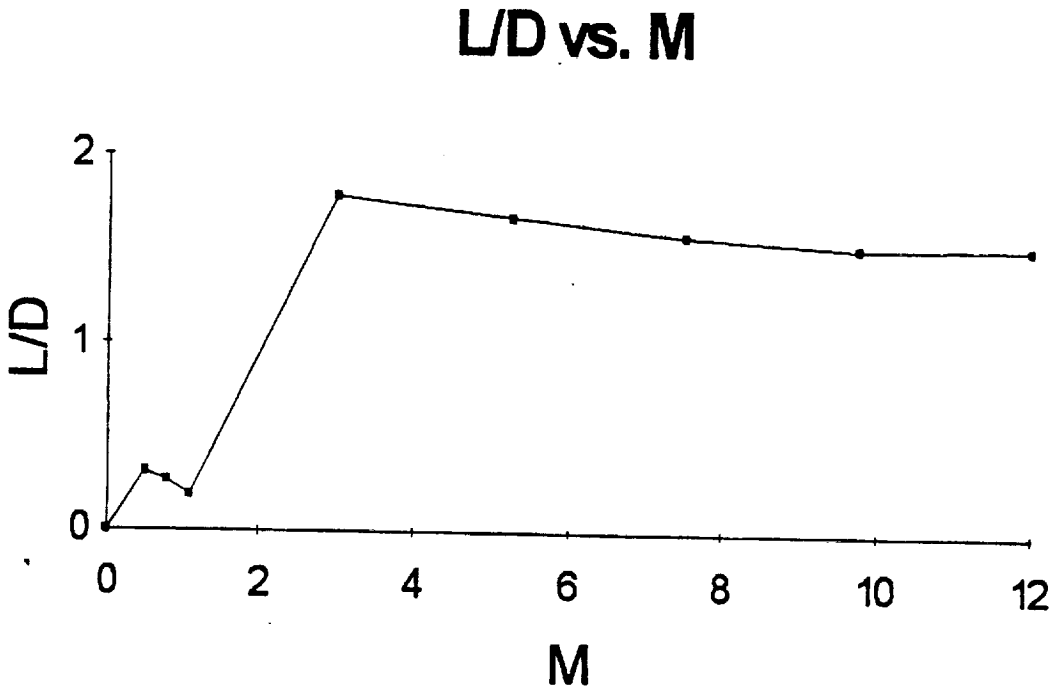

Figure 10: L/D vs. Mach number

Using three-dimensional cone theory would have given us higher lift and lower drag since the shock waves are weaker due to the extra degree of freedom for expansion (3-D relieving effect). Unfortunately, the Taylor-Macoll procedure for conical flow works in reverse. In other words, it calculates a cone angle based on a given shock wave. For this analysis it is necessary to obtain results based on a given cone angle. Hence, the reason for using the wedge becomes clear.

In an effort to keep our load factor low, the nose of the aircraft was changed from a boxed to a parabolic shape. This, along with shortening our wingspan, decreased the amount of lift our aircraft generated at low angle of attack. Consequently our load factor also decreased. Comparing Figures 11 and 12, it can be seen that the load factor, n, vs.

angle of attack curve shifts down after the nose is made parabolic. This allows for a larger range of angles of attack at which the aircraft can be flown without causing unnecessary stress on the aircraft structure.

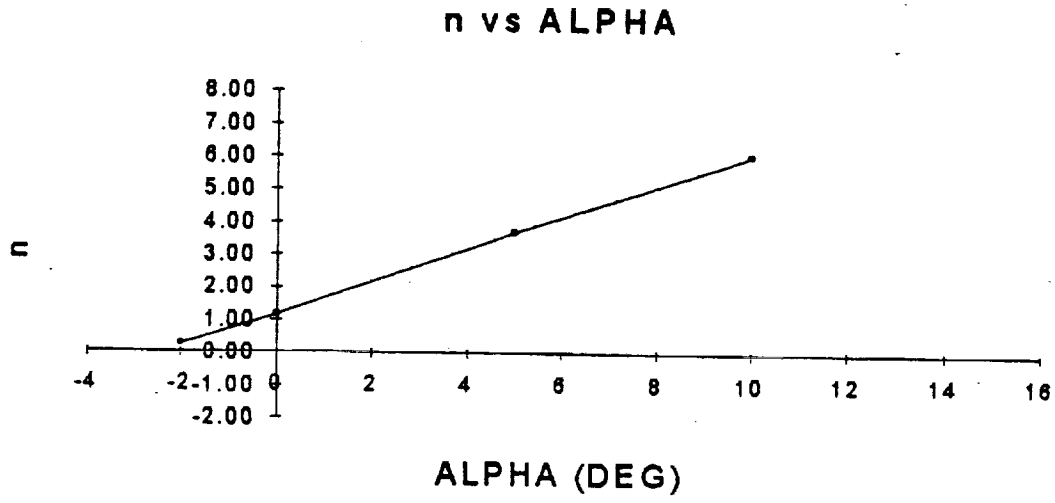

Figure 11: Load factor vs. ALPHA (rectangular nose)

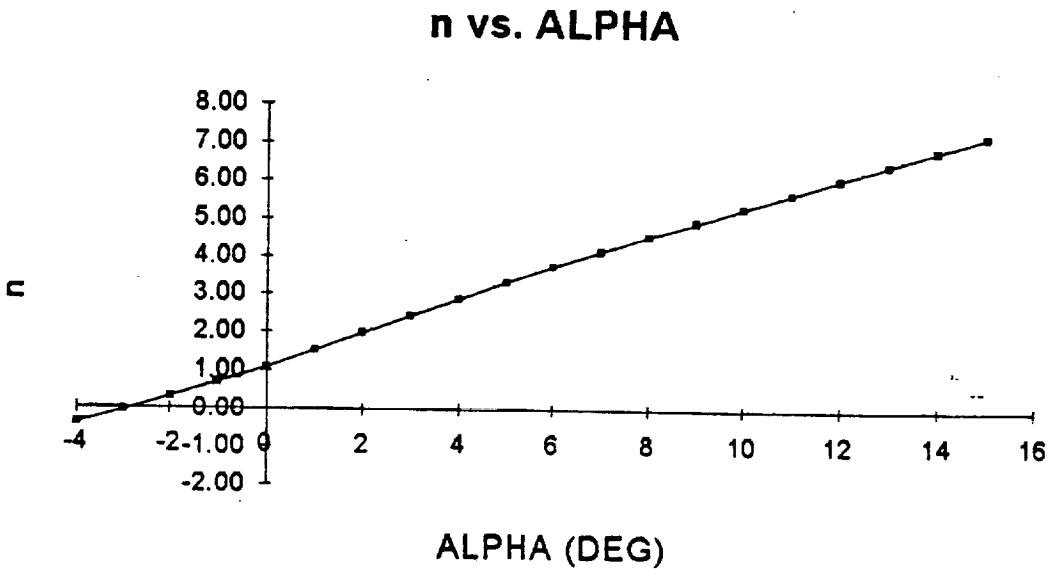

Figure 12: Load factor vs. ALPHA (parabolic nose)

Because our aircraft is lifting body, the entire cross-section of the body and not just the wings alone contribute to the calculation of the planform area, S. For this aircraft the planform area used to calculate the dynamic pressure, Q, at 120,000 ft. and Mach 12 is 95

ft.^{2}. Using this value of Q, the C_L vs. ALPHA curve which is shown in Figure 13 is obtained. The range of angles of attack is -5° to 15°. Higher angles of attack could not be tested due to the nature of the Prandtl-Meyer expansion routine in the computer code that was used in the analysis. It should be noted that the code also did not model boundary layer phenomena such as separation.

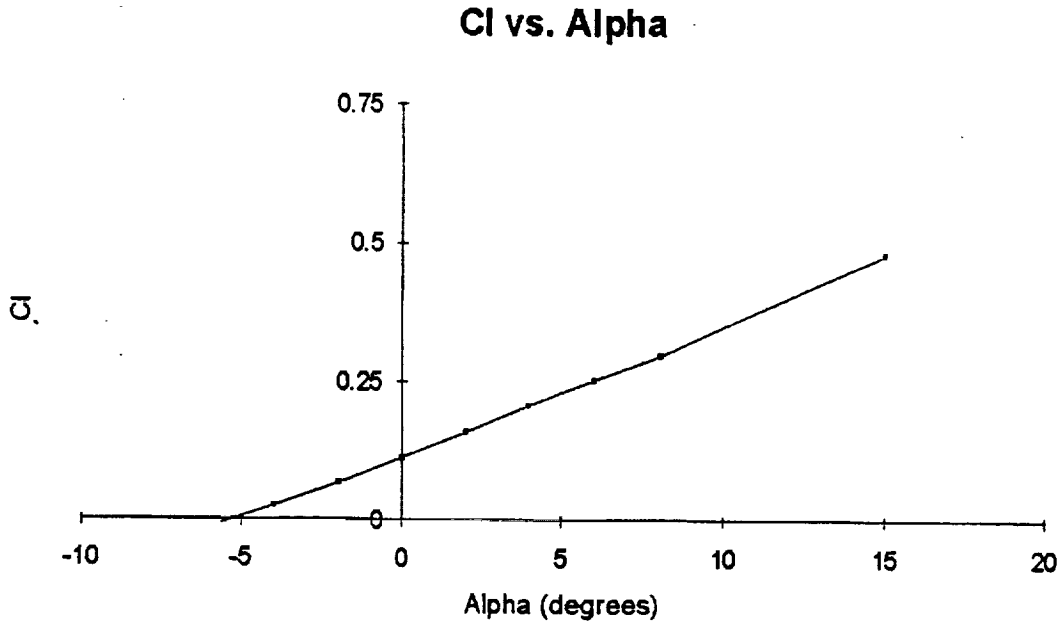

Figure 13: C_L vs. ALPHA

In conclusion, from a preliminary aerodynamic standpoint, this aircraft is capable of completing the assigned mission.

4. Trajectory

The trajectory was one of the most difficult problems faced by the design team. Our goal was to come up with a viable way of missile launching our aircraft using already existing technology. Two missiles were chosen as possible candidates to achieve our goal of 120,000 feet at a speed of Mach 12. These two missiles were the Minuteman and the Peacekeeper. This section will be divided into two major headings. They are:

- Analyis
- Results

Analysis

The analysis of the trajectory was performed using kinematic theory. From Newton's second law we have:

$$\sum F = M\frac{dV}{dt}$$

where M = mass at any instance of time, dt

V = velocity

F = forces acting on the system

Our analysis began with assuming a simple vertical launch and straight up trajectory. For this case, the forces acting on the system can be represented as:

$$M\frac{dV}{dt} = T - D - Mg$$

where T = Thrust of the rocket

D = Drag

g = Gravitational constant

and this can be broken down into an incremental equation for velocity:

$$V_2 = V_1 + \frac{(T - D)\Delta t}{M} - g\Delta t$$

This equation must now be examined closely. The thrust, drag, and mass of the system change throughout the course of the flight. The thrust of the rocket is a function of the altitude because assuming ideal expansion the thrust will increase with altitude because chamber pressure to atmospheric pressure increases. The drag changes with both the velocity and the altitude. The mass changes with time. By time stepping through the flight, the thrust can be determined as a function of time by determining the system position as a function of time. The drag can also can be found as a function of time by determining the operating conditions of the system at each time step. Now that the new velocity has been determined as a function of time only, the time dependent new altitude and the acceleration required to achieve this new velocity can be determined.

This is how the primary launch data of the rocket was determined at any instance in time. A time interval of 1 second was specified to obtain fairly accurate results.

The drag on the rocket was determined using the NASA Special Publication Number 3004 Tables for the Flow over Supersonic Cones at Zero Angle of Attack and calculating the skin drag on a cylinder approximating the maximum diameter of the system. These values were easily calculated above Mach 1.5. Below this, local subsonic regions would occur and we were unable to calculate properties in these regions. Since the system is subsonic for such a short period of time, a linear aprroximation for the lift was used below Mach 1.5 as Mach number increased.

Once this program was deemed to work properly, this ability to gimble the rocket nozzles was employed to change our trajectory to achieve the desired 120,000 feet altitude. In working with the propulsion group, it was determined that the optimum booster to

accomplish our goals was the first and second stage Minuteman ICBM. This new parameter meant that the drag, thrust, and weight would change nonlinearly during the transition from the first to the second stage booster. This was accomplished by using two separate time loops to examine each phase. This multistage trajectory also meant that the gimballing could be manipulated to take advantage of the combination of the lower acceleration at lower altitude and also the longer time to climb that comes with using two stages instead of one.

Results

There wre a few discoveries made while using the above analysis. First, we had to make sure that we did not give too large of an impulse to the system or the system would begin to tumble along its trajectory. Second, we needed to make sure that we lost as much momentum in hte vertical direction (rate of climb newarly zero) by the time we reached our test altitude or it would be very difficult to slow the aircraft down in the thin atmosphere. Third, our biggest constraint was our burn time. We had less than 2 minutes in which to accelerate to Mach 12 at an altitude of 120,000 feet.

Much of the trajectory was trial and error. We varied the gimballing until we obtained an desirable combination that left us at good separation conditions. We finished burning the first stage booster at 43000 ft and Mach 6. This speed is a little higher than desired for such a low altitude, but since the test vehicle is protected by the sheath, there is no danger. The second stage booster and sheath are then discarded at 123000 ft and at Mach 13.5. This higher speed and Mach number are necessary because the plane will descend and slow when the sheath is opened and in the delay until the scramjet engine is lit.

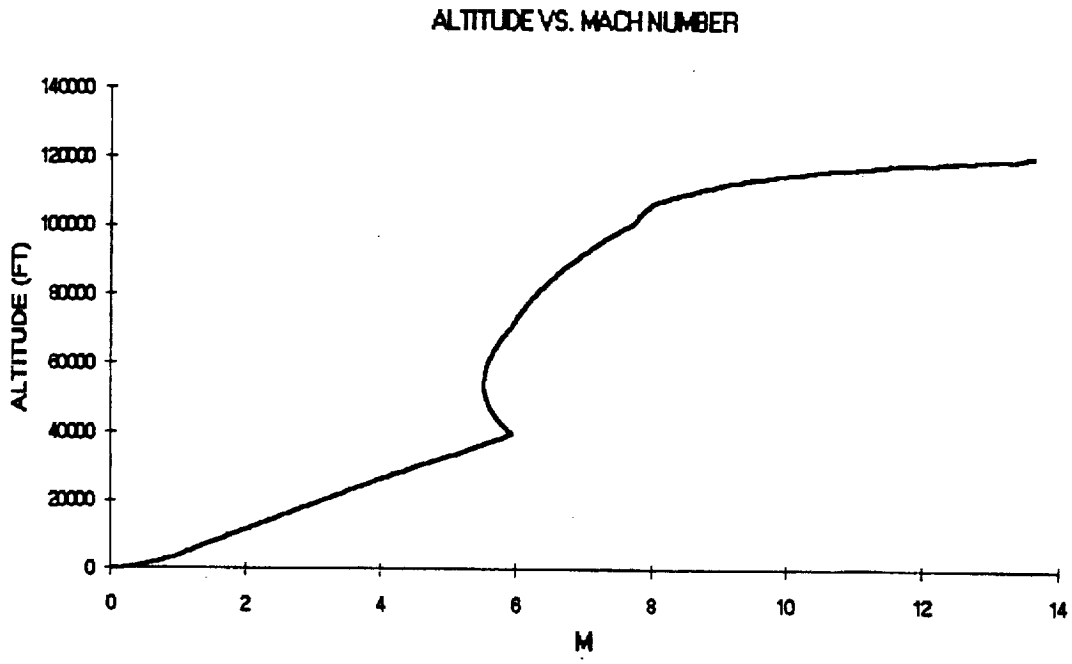

Figure 14: Altitude vs. Mach Number

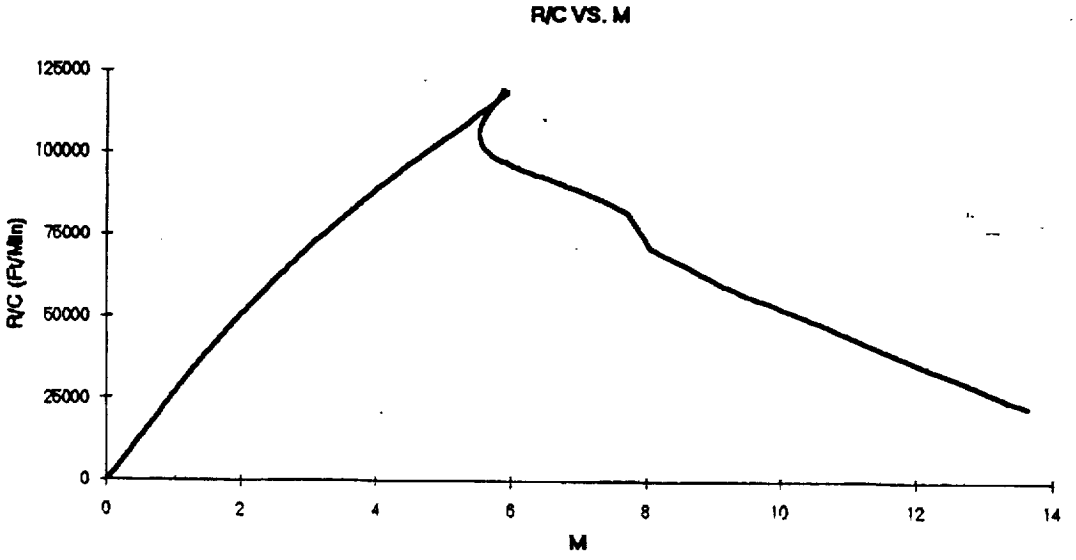

Figure 15: R/C vs. Mach Number

As shown in figure 15, when the aircraft is separated from the booster, we see that there is still a rate of climb (R/C) that must be dealt with. This will be accounted for with the opening of the sheath. While this area has not been thoroughly studied, it is expected that the rate of climb, the excess altitude and the excess speed will all be accounted for by this action.

The horizontal distance covered in this complete trajectory is extensive (Figure 16).

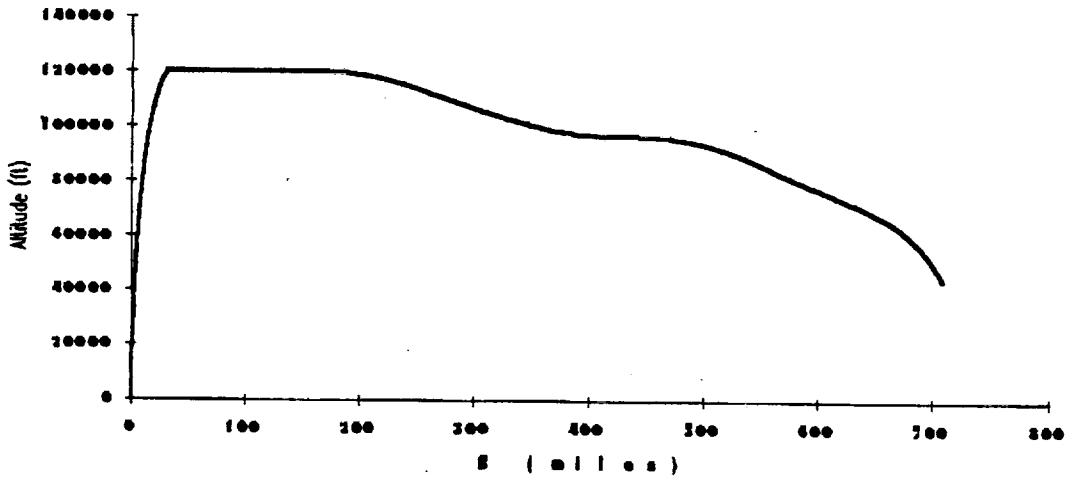

Figure 16: Altitude vs Distance

In order to reach the required 120,000 ft altitude, the trajectory covers 31 miles horizontally. The actual one minute test of the scramjet at Mach 12 will take about another 130 miles. At the conclusion of the test the scramjet will be shut down and the plane will glide down to Mach 2.5 (Figures 17 and 18) where the vehicle will be pulled up to stall. The glide phase of the trajectory will cover approximately 550 miles. This means that the total mission distance (excluding the parachute drift from 40,000 ft down to the ocean) is about 711 miles.

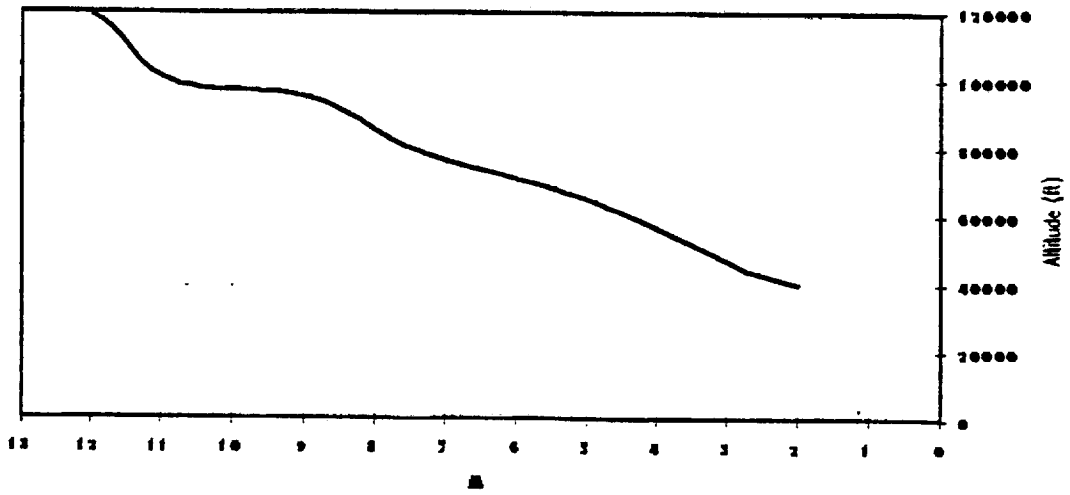

Figure 17: Altitude vs Mach Number

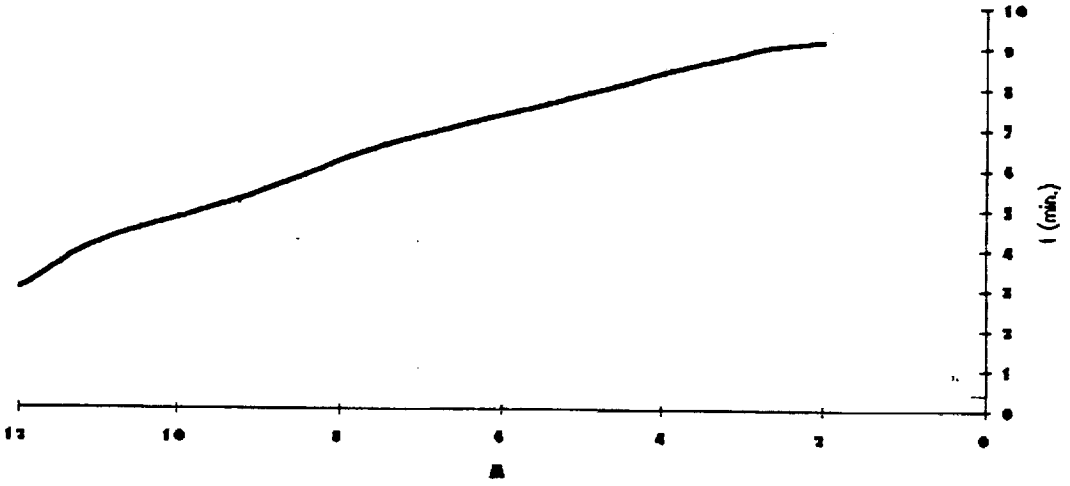

Figure 18: Mach number vs time

A recent adjustment to the decent trajectory was made. At around Mach 2, the vehicle will perform a 4g pullup. Upon stall, a rear parachute will eject that has a diameter of 50 feet. This will slow the vehicle enough to allow for a moderately hard water landing

that will not cause damage. Once the vehicle hits the water, a flotation device will deploy and keep the vehicle afloat until it is retrieved.

The methods used to control our trajectory appear to be reasonable and leave us with good results. Some improvements or changes could be to:

- Experiment with different descent trajectories
- Due more work on the booster and sheath disposal effects

5. Stability and Control

The pitching moment of the aircraft can be determined as shown in the aerodyanmic section of this report using equation (21). The results are plotted in Figure 19 with the moment coefficients based on the length of the aircraft and the planform area.

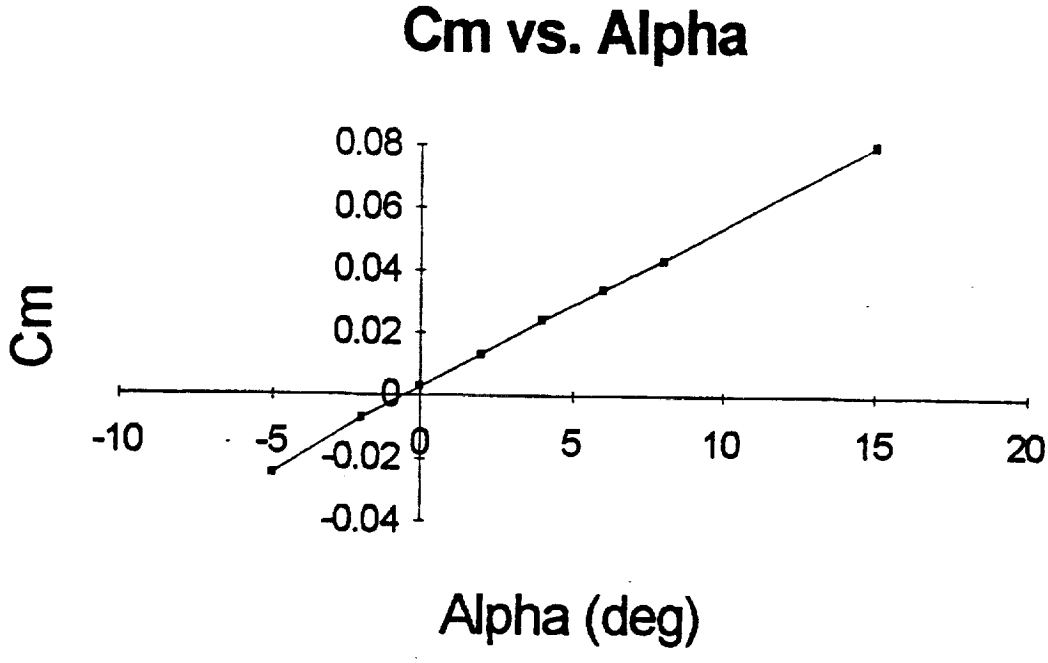

Figure 19: Cm vs Alpha

As you can see, the aircraft is unstable. The percent static margin for this aircraft was determined from the slope of this graph and the C_l vs. Alpha graph using the equation:

$$\frac{dC_m}{dC_l} = (h - h_{np}) \equiv \text{static margin} \qquad (32)$$

where h = percentage of chord location of the c.g.

h_{np} = percentage of chord location of the neutral point

The static margin was determined to be 14.314%. This is clearly highly unstable, but we feel it is correctable. The instability results from the large external diffuser in the front of the aircraft which provide most of the lift and the location of the center of the gravity behind this diffuser causing a large upward pitching moment. A possible means of correcting this would be to increase the upper surface deflection in the front of the aircraft to create a stronger oblique shock at the nose on the upper surface. This would create a higher pressure region and help to keep the nose of the aircraft down, but would result in higher nose temperatures. Another possible means of correcting this problem would be to install a canard near the nose of the aircraft at a negative angle of attack in front of the neutral point. The negative lift provided by this surface would create a negative moment to help counterbalance the positive upward pitching moment of the diffuser.

Vertical Tail Design

For the given final wing and body configuration, the vertical tail shapes were determined from the tail volume coefficient equation:

$$Cvt = lvt*Svt/Sw*b$$

where Cvt is the vertical tail volume coefficient, lvt is the length between the center of gravity of the entire aircraft and the MAC of the vertical tails, Svt is the vertical tail planform area, Sw is the wing planform area, and b is the wingspan. The tail volume coefficient designed for and suggested in class is 0.095. The lvt was initially estimated and then finalized after an iterative process to be 5.97768 feet. Solving for Svt, the area for both vertical surfaces is 23.73 feet squared.

Published reports on hypersonic vehicle design point to a leading angle of 70 degrees for protrusions from hypersonic vehicle bodies. Now using the following three design parameters; vertical tail the area of 20.1 feet squared, a vertical tail height of 4 feet, and a leading edge sweep of 70 degrees, the following dimensions for each vertical tail were calculated to be:

Croot	6.8
Ctip	2.00 ft
height	4.00 ft
t/c (4 degree half angle)	6.99927 %
L.E. sweep angle	67.0225 degrees
l	.1749215

Table 6: Wing Data II

6. Propulsion

As you know, the mission specifications require that the vehicle be missile launched and therefore one must consider the scramrocket. The principal behind the scramrocket is that a solid propellant is first used as the fuel for launch and at some later point in the mission (when all of the solid propellant is burned) a liquid propellant takes over as the fuel. The solid propellant can either be packed into the combustion chamber of the scramjet (supersonic combustion) or a canister with the solid propellant can be placed into the combustion chamber (see Figure 20). The benefit of the canister is that it can be ejected and that the walls of the scramjet combustion chamber and exhaust nozzle will be clean of any residue left by just packing the solid propellant into the scramjet and burning it. Soon after investigating how much thrust the vehicle needed for launch and to get the vehicle up to Mach 12 at 120,000 ft altitude, the scramrocket was ruled out due to the enormous amount of solid propellant needed. The scramjet would be very large to house all of the solid propellant for launch and for the acceleration to Mach 12 and would not be feasable for this specific mission.

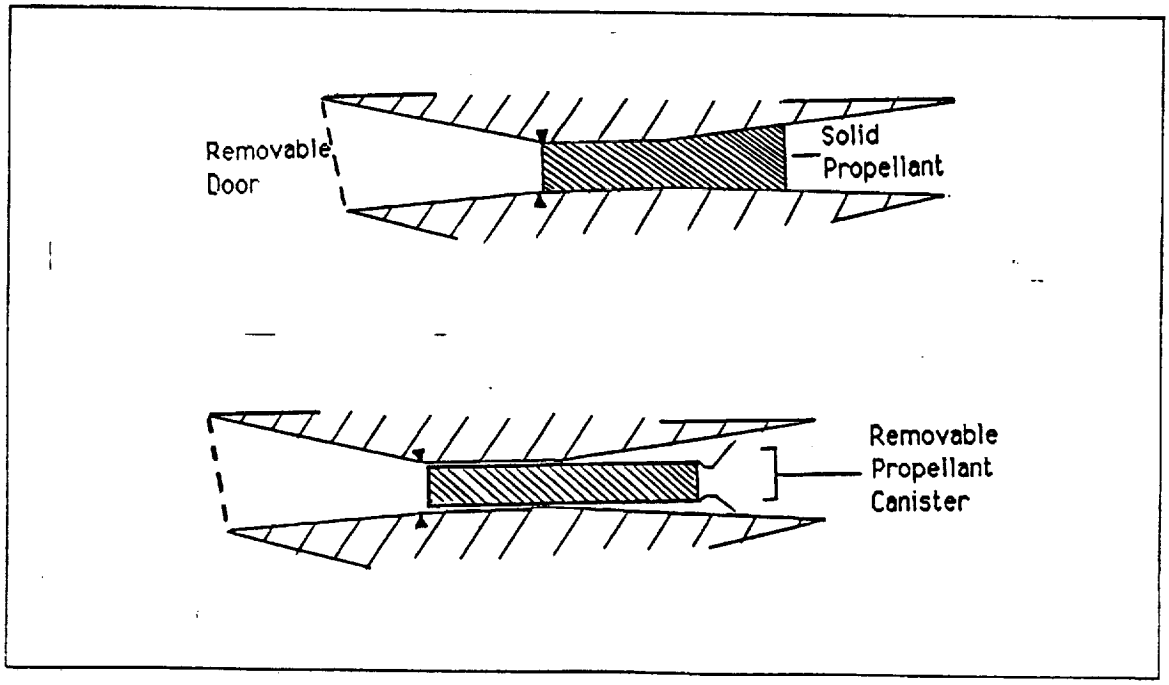

Figure 20: Scramrocket (packed in chamber and canister option)

Another scheme was to have an external booster combined with the scramrocket. The external booster would be used for launch and then at some point in the trajectory the scramrocket would kick in and take the vehicle up to Mach 12 at 120,000 ft. This idea was ruled out due to the complexity of having two rockets when really the external boosters could do the same thing and would cost less. So, the system of having external boosters for launch and the climb to 120,000 ft. at Mach 12 in combination with the air breathing scramjet turned out to be the optimum scheme for the mission.

The first area one must consider when investigation the air breathing scramjet is the type of fuel to be burned. Fuels considered were JP, methane, hydrogen, and fluorine. Fluorine turned out the be the ideal candidate due to its very high specific impulse (Isp) but cannot be used due to it being highly poisonous, corrosive, and difficult to handle (Anderson, pp510). Therefore, fluorine was quickly ruled out for the fuel for the scramjet engines due to the environmental issues at hand. As you can see in Figure 21, the heat capacity per pound is relatively low for JP and methane but is very high for hydrogen. This makes hydrogen a very likely candidate because it can absorb a tremendous amount of heat per pound. Therefore it could also serve as a heat sink for the hot points on the vehicle such as the leading edges of the wings and vertical stabilizers, nose, engine, nozzle, etc. On the other hand, Figure 22 shows that the heat capacity per unit volume is low for hydrogen as compared to JP and methane. To use hydrogen, more volume for housing the fuel would be needed which means a larger vehicle both in size and weight.

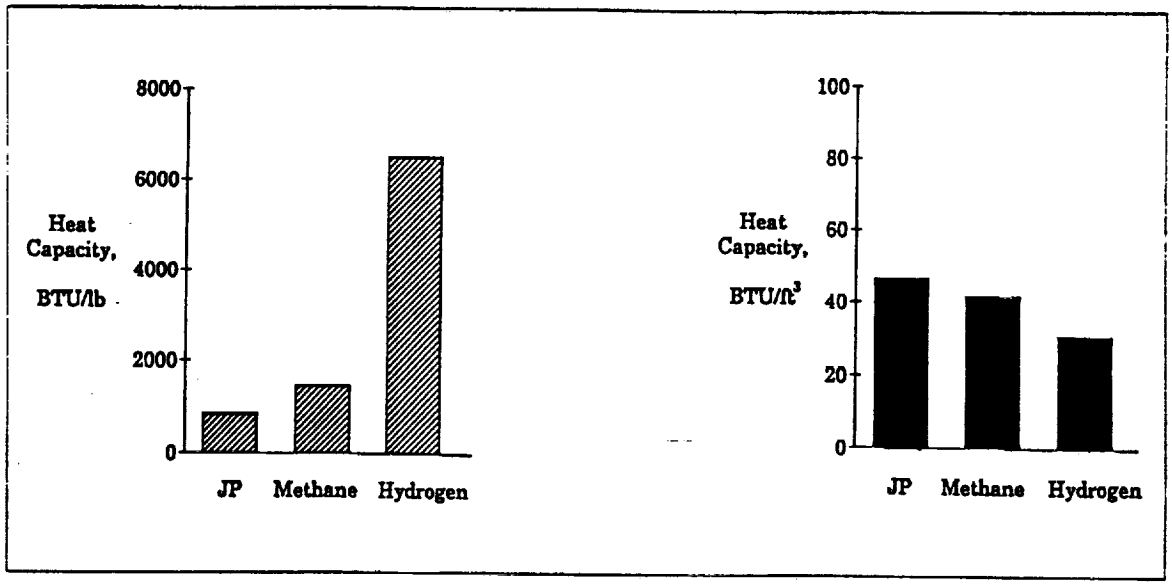

Figure 21: Heat Capacity (BTU/lb.).

Figure 22: Heat Capacity (BTU/ft^3).

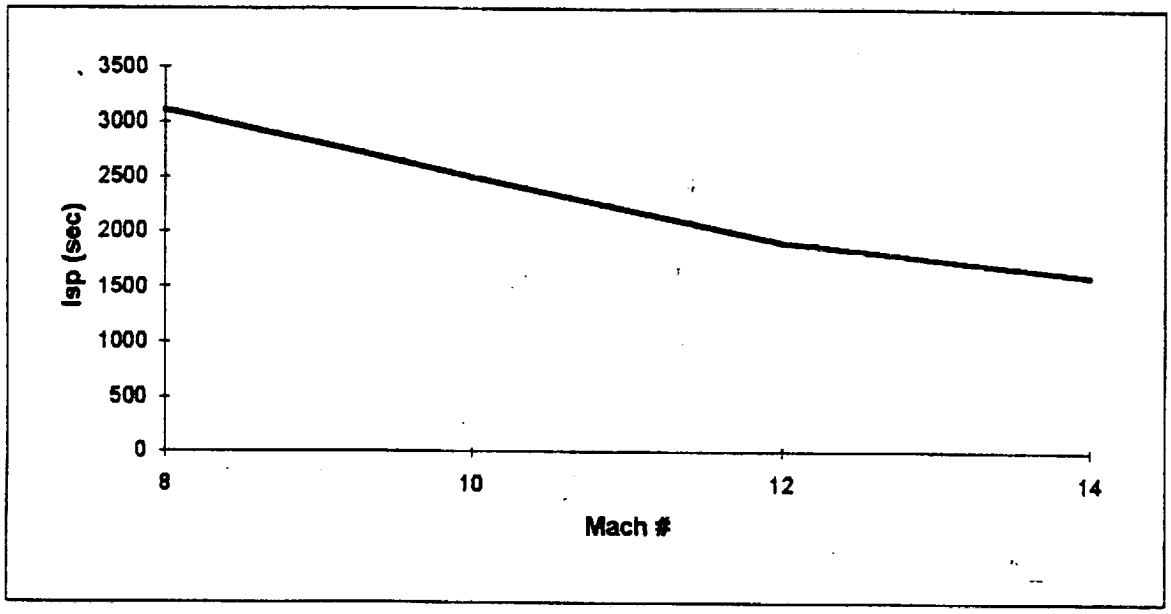

Figure 23: Specific Impulse vs Mach Number

Figure 24 shows that for a vehicle traveling at Mach 8-16, hydrogen is the only fuel which can be used for an air breathing engine. Hydrogen, as stated earlier, can be used for both the fuel for the scramjet and to cool the hot spots. Although hydrogen has a low density (more volume needed) the extremely high Isp is very favorable (Sin-I, pp184). In

addition, hydrogen is a clean burning fuel which does not coke the walls of the combustion chamber and/or the exhaust nozzle. Hydrogen's low flame radiation means cooler wall temperatures (Transportation, pp 60). Therefore, hydrogen will be the fuel used for our test vehicle traveling at Mach 12 at 120,000 ft.

With hydrogen as the fuel for the scramjet, a few programs were looked at which were written by Dr. Edse. The first program written in FORTRAN assumes a normal shock at the inlet of the scramjet and the second program written in BASIC assumes an isentropic diffuser. The normal shock assumption quickly showed that the highest Mach number attainable (even with a combustion Mach number of 1.1) was 10. With a combustion Mach # as low as 1.1, the pressures and temperatures are enormous and the vehicle would melt or explode before any test data could be recorded. The normal shock assumption was the extreme case and cannot be used since our specifications are for a Mach 12 freestream scramjet test. The program for the isentropic (dS=0) assumption follows the scheme depicted in Figure 25.

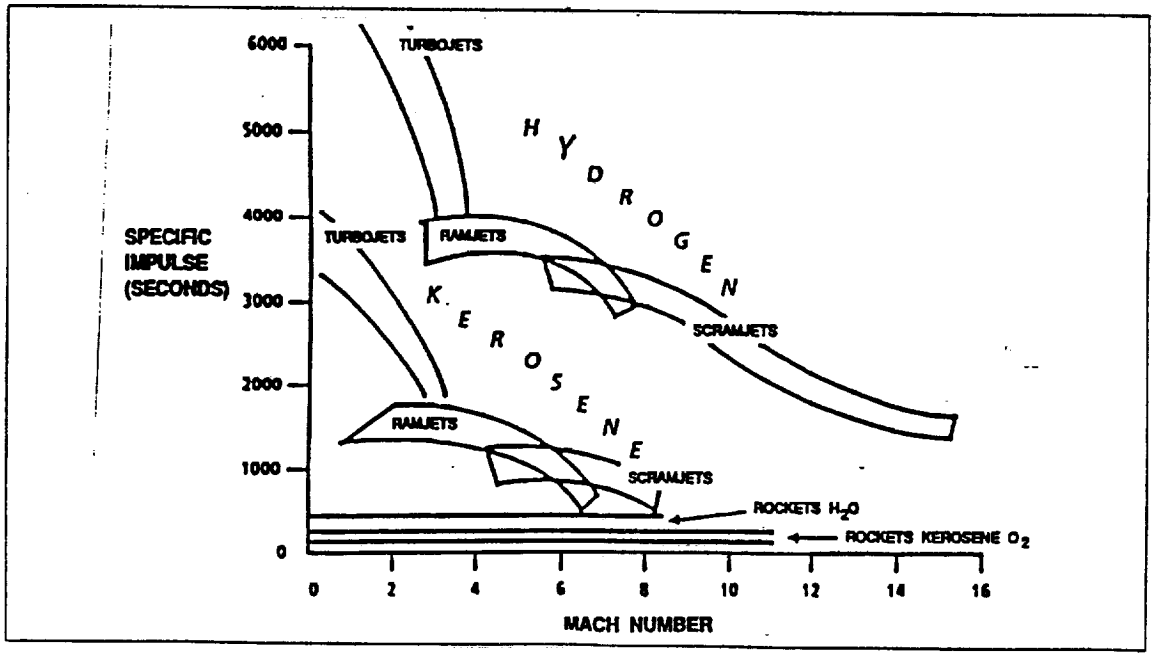

Figure 24: Hypersonic Propulsion Cycle Performance (Glassman, pp 8)

loop 1: The composition of the combustion gas is calculated by means of the condition that: $f_{O2}^{calc} = f_{O2}$ and $f_{N2/O2}^{calc} = 3.76$

loop 2: Tc is obtained for the condition that $(h_f / \Re)^{Tc°calc}_{CG} = (h_f / \Re)^{Tc°}_{CG}$

loop 3: The composition of the dissociated air at the diffuser exit is obtained from the condition that: $f_{N2}^{calc} = 3.76$

loop 4: P_{de} is obtained from the condition that $(s / \Re)^{Tde}_{eq\ air} = (s / \Re)^{T\infty}_{air} + (\Delta s / \Re)$

loop 5: T_{de} is obtained from the condition that $u_{de} = u_{de}$

loop 6: P_c is obtained from the condition that Ac = Ade + Af and $P_c^{calc} = P_c^{est}$

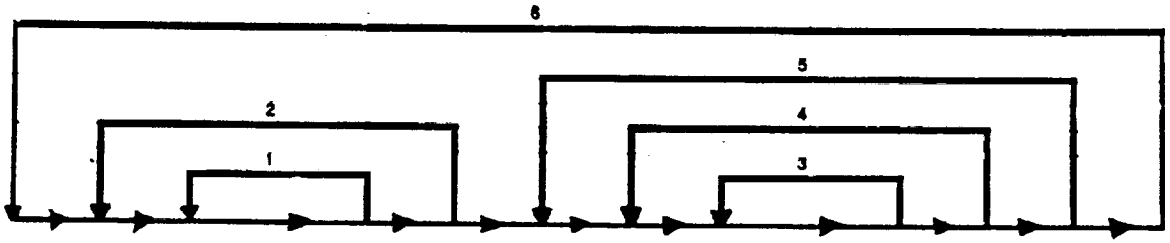

Figure 25: Scramjet Combustion Chamber Iteration With Mc Specified (Edse)

The calculation of the diffuser exit conditions are based on the following conditions and assumptions:

1.) The deceleration of the air entering the diffuser is adiabatic.

2.) Thermodynamic and Chemical equilibrium prevails everywhere in the diffuser at all times.

3.) The freestream conditions are known: T∞, P∞, Mf

4.) Air consists of one mole of oxygen (MM_{O2} = 31.9988 kg/mol) and 3.76 moles of nitrogen (MM_{N2} = 28.0134 kg/mol) such that MMair = 28.85067 kg/mol.

5.) The diffuser exit speed ude as well as the diffuser exit Mach number, Mde, can be calculated only when the combustion chamber exit Mach number, Mc, is specified.

An efficiency of the diffuser can also be specified. For all calculations, a diffuser efficiency of 80% was used.

The combustion chamber was assumed to be of constant area ($dA = 0$). From a theoretical point of view the optimum performance of the exhaust nozzle of any jet engine is obtained when it is designed to expand the propellant gas to the pressure of the ambient atmosphere ($Pe = P\infty$). However, for high pressure ratios such an expansion may lead to extremely large exit areas and thus long and heavy exhaust nozzles. Therefore, the actual performance of the engine may be reduced because of the extra weight and drag of such large nozzles. In Dr. Edse's program, ideal and isentropic expansion was assumed (Edse).

The results of the pressure and temperatures in the combustion chamber as a function of combustion chamber Mach number are shown in Figure 26 and 27 respectively. For optimum performance, one would wish to combust the gas in the combustion chamber at as low a Mach number as possible, as close to Mach 1.0. But the pressure and temperature at these low combustion Mach numbers are astronomically high and the scramjet will either explode or melt (Edse).

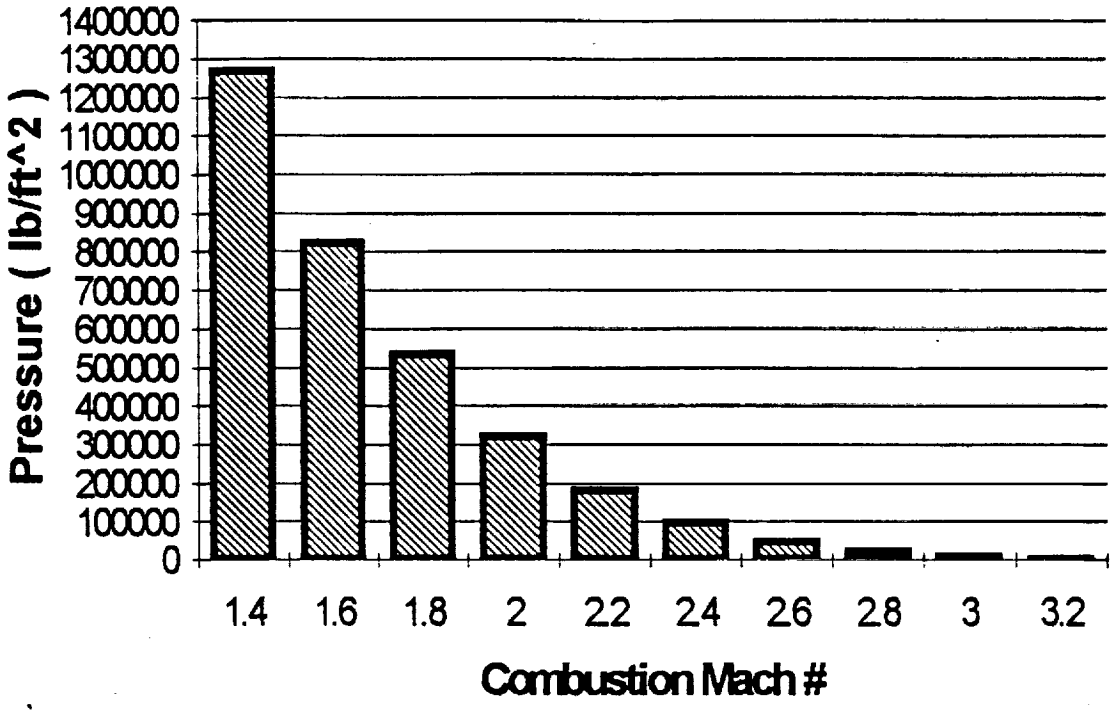

Figure 26: Pressure in the Combustion Chamber vs. Combustion Mach Number

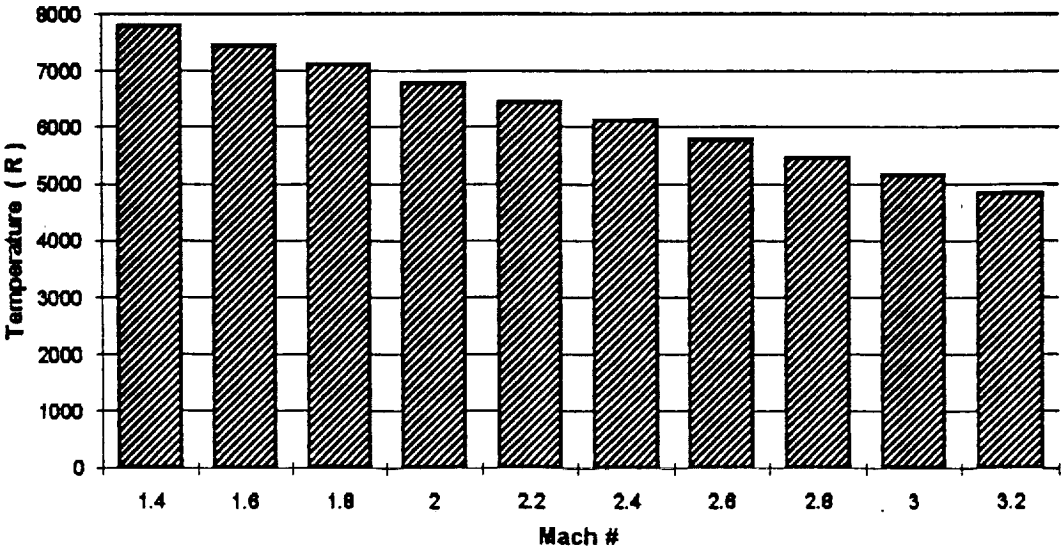

Figure 27: Temperature in Combustion Chamber vs. Combustion Mach Number

Scramjets can handle a pressure of approximately 160,000 lb./ft^3 and a temperature of around 6100 °R with active cooling (Edse). With this in mind, we see from the figures that the lowest combustion Mach number we can handle is approximately 2.4 - 2.8.

Dr. Edse's programs were very helpful to get the feel of how a scramjet works and rough ideas of how certain parameters change and how they interact with one another. GE Aircraft Engines ran tests on scramjets varing altitude, mass flow, free stream mach #, free stream velocity head, and static pressure ram recovery (see Figure 28).

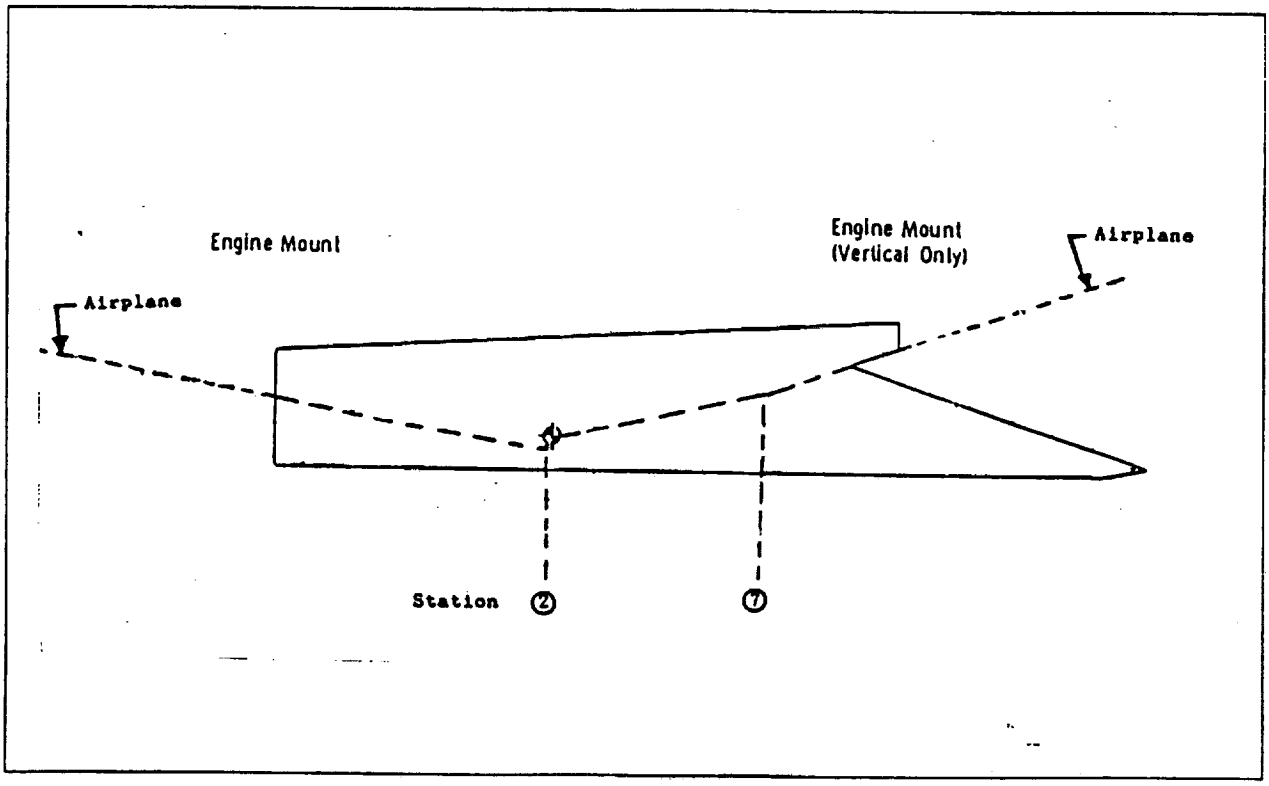

Figure 28: GE Scramjet - H_2 Fuel (GE Aircraft Engines, Advanced Technology Operation)

The engine performance for the GE scramjet tests give for a Mach 12 free stream, a 71 lbs/sec mass flow, an fuel / air equivalence ratio of 1.8, 13,396 lbs of gross thrust and 4,516 lbs of net thrust. The tests were done in 1990 and by the year 2000, we hope to see

a net thrust of approximately 4950 lbs with new technology and continued tests. The combustor pressure and temperature for this engine is 1800 lb/ft^2 and 1601 °R, respectively.

The total pressure recovery for the vehicle at a free stream Mach # of 12 is 0.82 (see Figure 29). The pressure recovery numbers given in the graph are up to the inlet to the scramjet. The numbers do not include the straightening of the airflow before the combustion chamber. If the straightening is to be acounted for, the total pressure recovery would be much less, in the area of 0.32.

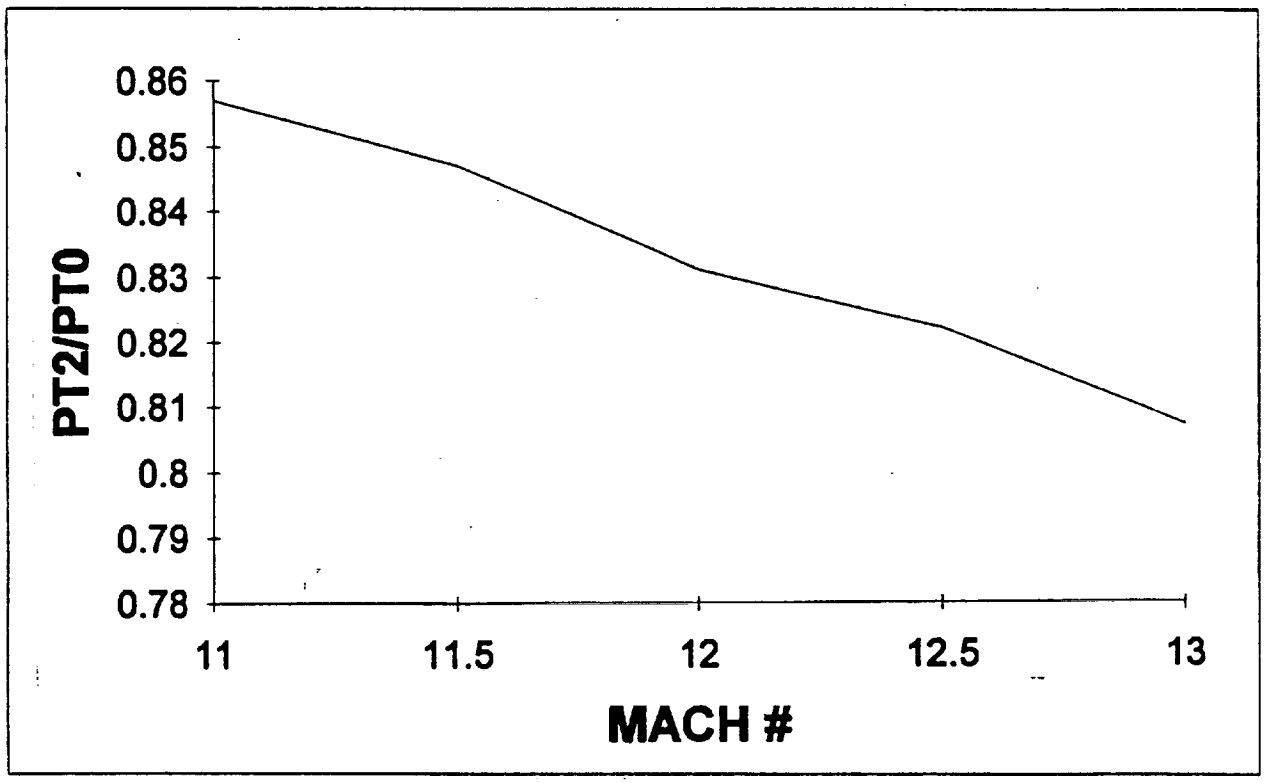

Figure 29: Total Pressure Recovery

The plans to further improve the scramjet performance is to investigate the exit nozzle. The current configuration requires one scramjet to overcome the drag at Mach 12 at 120,000 ft.

Since our design team had the option of using a rocket launch. it was decided that we would use rocket propulsion to get the aircraft all the way to the test altitude of 120,000 ft. and speed of Mach 12. Upon deciding to use a rocket launch, trade studies between solid and liquid propellants, one stage and multistage rockets, and existing rockets versus a new design were then conducted.

In comparing the solid and liquid rockets, a few major characteristics came to the forefront. The first of these was the ability to control the thrust of the rocket. With a liquid propellant rocket one can vary the amount of thrust by controlling the mixing of the propellant and oxidizer. This can be done in only a limited fashion in a solid propellant rocket by the type of grain configuration chosen. The ability to vary the thrust is important because it is desirable to have a lower thrust at the low altitudes to minimize the heating of the rocket and plane, and then have a very high thrust at the test altitude to accelerate the aircraft to the test speed.

The second major characteristic is a result of the first. The propellant in a solid propellant rocket is stored in the combustion chamber. In a liquid propellant rocket the fuel and oxidizer are stored separately and are transported to the combustion chamber for mixing and burning. This means that solid rockets are less complex, require less servicing, are more stable, and when comparing fuels, less toxic. In sum, the ability to vary the thrust of a liquid propellant rocket is offset by the added weight, complexity, and safety risks.

In comparing these two factors, it was decided that the solid propellant rocket was the better choice for this mission. Since the goal is to get a flying test bed to a certain height and a certain speed, a solid booster rocket seemed adequate when compared to all the added complexity of a liquid booster.

We next looked at the possibility of using an existing booster instead of designing our own. The incentive of doing this is by using an existing booster, it isn't necessary to invest a lot of money into the research and development, as well as the normal fabrication costs associated with developing a new rocket. The ideal booster rockets in existence were

found to be the military intercontinental ballistic missiles (ICBM's). These multistage stage rockets have boosters that range in thrust from 60,000 to 500,000 pounds of thrust.

We next looked at the burn rates of these rockets and as is typical with solid rockets, the burn rates were such that the total burn time of a particular stage is less than one minute. While this burn rate is necessary to produce the high thrust gained from the solid rocket booster (SRB), our particular mission doesn't compliment this characteristic at all. To use one stage would mean an exceedingly high thrust booster to acheive the acceleration necessary to reach Mach 12 in under one minute. This high acceleration is undesirable from a trajectory standpoint due to aerodynamic heating at the lower altitudes and control problems at the test altitude. We therefore looked into the possibility of a multistage booster so we could double the time spent to get to Mach 12 at 120,000 ft. This requires a lower thrust boosters and minimizes the trajectory problems. The decision we settled on was using the two stage Minuteman ICBM as the booster. The large thrust of the first stage is sufficient to get the system to Mach 6 at 43000 feet. The second stage is then emplowyed to get the system to Mach 13.5 at 122000 feet. By employing the gimballing feature on the nozzles, the trajectory can be controlled so the test vehicle is horizontal at the end of the boost phase.

One problem that still exists, however, is that of how to attach the test vehicle to the booster. Since the vehicle is so small, it was decided to attach it to the top of the second stage booster. By doing this, the rocket can more easily fly in its ballistic trajectory.

Another problem that existed was how to protect the test vehicle in the high Q range of the ballistic ascent. The best way to protect the plane would be to enclose it. A sheath was therefore devised. The sheath is a combination cone and cylinder that protects the entire test vehicle during the launch phase and then peals away prior to lighting the scramjet engines. The current design of the sheath is robust and can be downsized (Table 7). The material used in the sheath is the same as the Minuteman and is Ladish D6AC steel.

Cone half angle (degrees)	20
Cone length (ft)	11
Cylinder shell length (ft)	12
Total weight (lbs)	3000
Maximum diameter (ft)	8

Table 7: Nosecone Data

In conclusion it was decided that a two stage Minuteman booster was best suited to meet our needs. Its combination of high thrust and combined long burn time make achieving our goal of Mach 12+ at 120000 feet possible. The data on the Minuteman is given below.

Weight (less the nose cone)	(lbs.)	200,000
Burn Out Weight	(lbs.)	4264
Propellant Weight	(lbs.)	45,831
Length	(in.)	294.87
Outside Diameter	(in.)	65.69
Burn Rate	(in/sec)	.349
Burn Time	(sec)	53.5
Burn Time Average Thrust	(lbs.)	194,600
Action Time Average Thrust	(lbs.)	176,600
Propellant Volume	(in^3)	709,400
Average Burning Area	(in^2)	38,500
Propellant Density	(lbs_m/in^3)	.0636

Table 8: Minuteman First Stage Missile Data

Weight (less the nose cone)	(lbs.)	59,000
Burn Out Weight	(lbs.)	1445
Propellant Weight	(lbs.)	14,055
Length	(in.)	162
Outside Diameter	(in.)	52
Burn Rate	(in/sec)	.349
Burn Time	(sec)	57.5
Propellant Density	(lbs_m/in^3)	.0636

Table 9: Minuteman Second Stage Missile Data

These values are taken at sea level conditions, so the thrust will change altitude. If we consider the ideal case where the exit pressure of the rocket is equal to the atmospheric pressure, we can easily calculate the thrust variation with altitude by using the equation for specific thrust.

$$C_F=[2K^2/(K-1)*(2/(K+1))^{(K+1)/(K-1)}*\{1-(P_2/P_1)\}^{(K-1)/K}]^{.5}$$

Where K is the specific heat ratio

This relation yields:

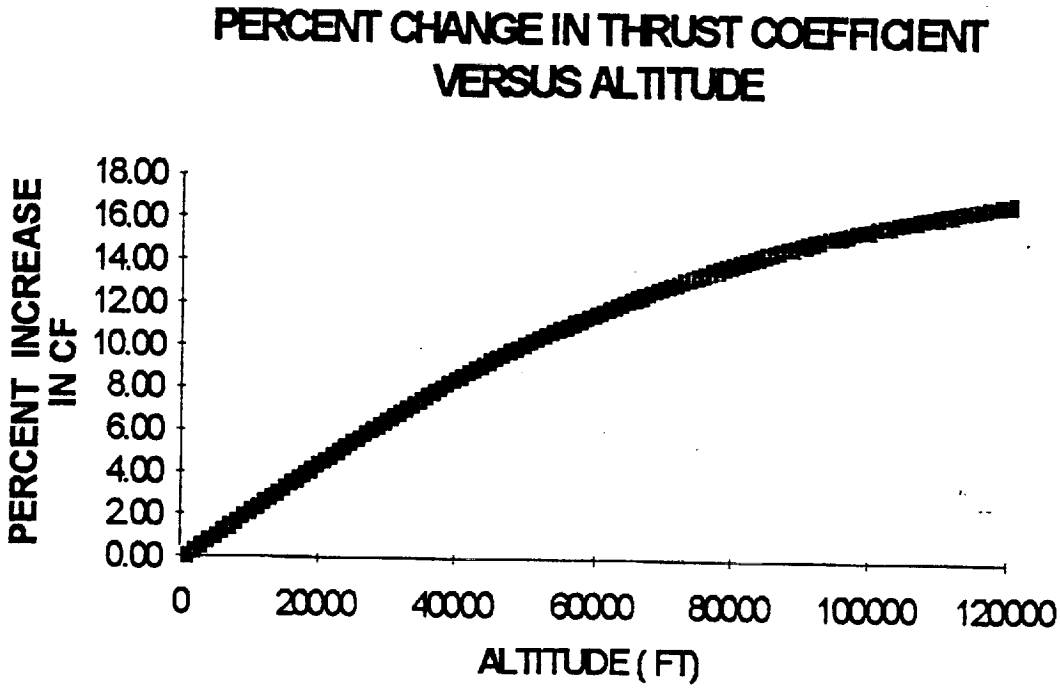

Figure 30: Thrust Coefficient vs. Altitude

As the altitude increases, the atmospheric pressure decreases. This causes the pressure ratio (atmospheric pressure to chamber pressure) to decrease and therefore yield a

larger thrust coefficient. As the rocket travels from sea level to 120,000 feet, this increase is 16.8 percent. This corresponds to a increase of 16,800 lbs. of thrust for the first stage booster. This is an important fact to be accounted for when determining the trajectory.

In conclusion, we chose the Minuteman for three reasons. The Minuteman is a solid rocket booster so it is easy to maintain and relatively safe. It is a production rocket so typical production start up costs don't apply. Lastly, due to the characteristics of the mission, it has the needed high thrust available and the second stage to increase our time to climb.

7. Weights and Volume

One of the most important parameters in the design of any aircraft is the weight. It is this parameter that drives the propulsion needs, aerodynamic requirements and, the cost of the design. During the optimization phase of design, it is important to look at ways to reduce the weight and keep it at a minimum while still completing the mission. This report, however, is concerned with the preliminary conceptual design phase, and covers only the estimation of weight and volume, not minimization.

The volume of an aircraft is also an important consideration. During conceptual design, systems are designed that require a certain amount of space within the vehicle. A designer who forgets to allow room for these systems, as well as fuel and payload, dooms his design to failure. For this reason, an accurate estimate of the vehicle volume and a working inboard planform are essential during the design process.

This report summarizes the methods used to estimate the vehicle weight and volume for the OSU II design. The results of these estimations are given in tabular form. Also, a preliminary inboard planform is given. Although the exact location of the various systems within the vehicle is open to change, the planform given was used to calculate the center of gravity (CG).

Weight Estimation Methods

The OSU II design system consists of one two-stage booster rocket and a test vehicle. It is important to know the weight of both the booster and the test vehicle. However, because the boosters being considered can be taken "off the shelf", no estimate of their weight is needed. Rather, we can simply use the known weight of the boosters along with the estimated weight of the test vehicle.

To obtain an accurate estimate of the vehicle weight, three methods were considered. NASA's Hypersonic Aerospace Sizing Analysis (HASA) is a fortran code that provides weight and volume estimates for user provided input parameters (Ref. 1). This

code can be extremely helpful during preliminary design, however, it is not set up to run our type of system. The modifications made to HASA, as well as results of those modifications, are discussed in a subsequent section. In addition to HASA, we employed a comparison method to obtain the vehicle weight. This method provided a fairly accurate weight approximation. Finally, the Wright-Patterson program PDWAP was employed to obtain a complete weight breakdown of all components.

The comparison method used assumes that vehicles designed for similar speed regimes and for similar applications should be roughly the same weight for a given size. If this assumption is accepted, the designer who knows his own vehicle's size need only obtain weight and size information for existing aircraft to obtain his design weight. This is the method that was used.

The Boeing Beta Orbiter (Ref. 2) and the Space Shuttle were selected as comparison aircraft. The Boeing orbiter was used mainly because detailed weight and size information was available. The Space Shuttle was chosen as the result of a trade study of comparison vehicles (Ref. 1). Parameters indicative of vehicle size and weight were considered for several vehicles. The values were compared to the known or anticipated design parameters to determine the comparison vehicle most like the design (See Table 10).

Aircraft	Rockwell	Hycat-1A	Hycat-1	**Shuttle**	Gen. Dyn.	**Design**
W/S	**51.64**	67.5	88	82.2	500.7	47
Mass Frctn	.3178	.3488	.3709	**.1274**	.7092	.1
Aspct Rto	**1.357**	**1.357**	**1.357**	1.961	12.12	.971
T/W	.48	.5	.5	5.53	**1.66**	1.09
t/c	.03	.03	.03	**.11**	.21	.087
Taper Rto	.145	.154	.099	**.2**	.8	.35

Table 10: Comparison Model Trade Study
****Bold face indicates parameter close to design value**

Thus far, the word "size" has been used rather casually. This is because the meaning of "size" in the comparison method used depended upon the vehicle component being analyzed. For example, to determine the wing weight, the ratio of Space Shuttle wing weight to wing area was formed and multiplied by the design wing area. Likewise, the payload bay weight was found by matching the ratio of bay weight to bay volume for the Beta Orbiter. Thus, the size used varied for each component. This method was used for all structural weights, the payload bay weight, and the weight of the fuel tanks. Some components, however, had no obvious characteristic size.

The weight of the thermal protection system (TPS), avionics, and electronics could not be determined using a weight to size ratio. Therefore, another method had to be employed. To determine the weight of these systems, equations were extracted from the HASA fortran code. Although the code is an iterative process, some of the equations depend only upon final values of the vehicle gross weight, surface area, volume, etc. The TPS, avionics, and electronics weight equations were of this type. For this reason, we needed only to use our known design parameters in these equations.

The propulsion system was not analyzed using either method outlined above. The weight of the scramjet engines was taken from General Electric engine data (Ref. 14). Also, the weight of liquid hydrogen necessary for the one minute cruise was supplied by the propulsion group. The results of the weight estimation for the test vehicle are given in Table 11. The total system weight is obtained by adding the weight of the Minuteman two-stage booster rocket to the test vehicle weight. Each first stage booster weighs 50,000 lbs, while the second stage weighs 15,500, bringing the total system weight to 76,600 lbs. 3000 lbs has also been added as the weight of the sheath.

Finally, the entire weight breakdown was reanalyzed using the PDWAP code. A high speed lifting body data file was given with the code, and the inputs were modified to satisfy our design. The main components such as engine weight, structural weight, and fuel mass were given as constants. PDWAP then gave specific weightsof the avionics,

electronics, fuel system, and several other components. It also perfected the weights of our given inputs. A detailed breakdown is given in Table 11. As it shows, the total vehicle weight without booster comes to 7223 lbs.

Component		Weight
Aero Surfaces		302
Wings	157	
Vertical Stabilizers	145	
Body Structure		2134
Basic Body	1542	
Secondary	470	
Thrust	122	
Thermal Protection System		570
Propulsion		1256
Scramjet	906	
Fuel Tank Insulation	60	
Fuel System	129	
Pressurization System	110	
Recovery Gear		303
Avionics		1071
Electronics	146	
Hydraulics	103	
General Controls and Avionics	376	
Attitude Controls	189	
Aerodynamic Controls	326	
Vehicle Dry Weight		5636
Payload		1000
Main Propellants		450
Reserve Propellants		138
Vehicle Total Gross Weight		7223

Table 11: Weight Results

A weight vs. time comparison can be made because the burn rate, burning area, fuel density and burn time of each stage of the Minuteman is known. The burning is assumed to be held constant so that the following equations can be used to determine the propellant weight of each booster stage:

$$Burn\ Rate\ x\ \ Burning\ Area\ x\ \ Fuel\ Density\ =\ Fuel\ Flow\ Rate$$

$$Propellant\ Weight\ =\ \ Fuel\ Flow\ Rate\ x\ \ Burn\ Time$$

Also, because the burning area, burn rate and fuel rate are constants, the system weight varies linearly with time throughout the burn time of the boosters. Once the first stage runs out of fuel, it is dropped off (as is the second stage) so that the system weight becomes the fully fueled test vehicle weight. Once again, as an approximation, the fuel flow rate through the scramjet engines is assumed to be constant. Therefore, through the one minute burn time, the system weight decreases linearly by the weight of enough liquid hydrogen to power the three scramjets for the test period. At the end of the test period, the fuel has expired and the system weight, which is now the empty weight of the test vehicle, remains constant. Figure 31 shows calculated values for weight vs. time.

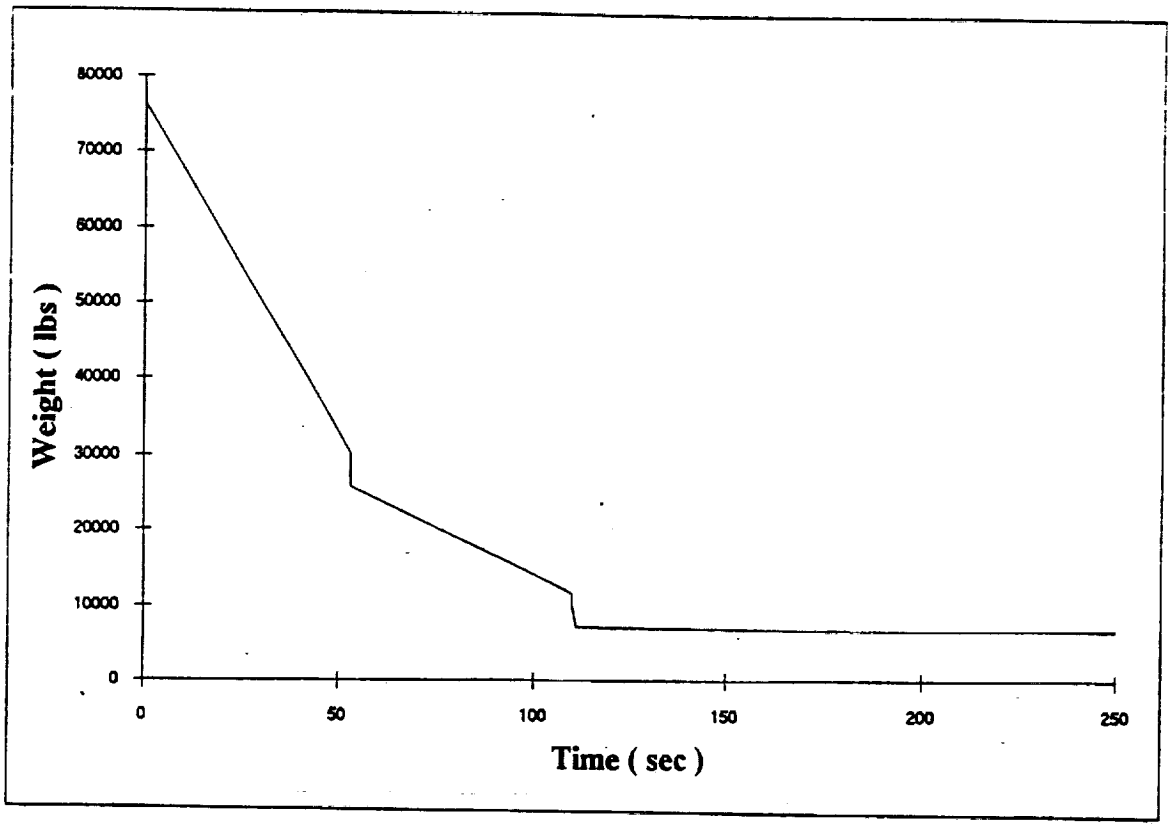

Figure 31: Weight vs. Time

After the first two weeks of the design project, our test vehicle design was 150 feet long with a wing span of close to 60 feet. This oversized design caused considerable booster problems. The test vehicle was then downsized to a length of 35 feet and the new weight estimate, based in part on an structural approximation, was 20,000 lbs. In trying to further optimize our design, we again downsized to 20 feet. The new weight estimate came to about 7500 lbs; however, PDWAP showed a total weight of 7223 llbs. Due to the comprehensive nature of PDWAP, we decided to use this value as our final weight.

Volume Estimation Methods:

Again, because the specifications of the booster rocket are known, no estimation of its volume is necessary. The volume of the test vehicle was broken down into three parts: fuselage volume, wing volume, and vertical stabilizer volume.

The fuselage volume was determined by breaking the fuselage into easily analyzed component pieces and summing the component volumes. The preliminary design fuselage has a constant longitudinal cross section. That is, the cross section does not vary from one wing root to the other. This was helpful in the calculation in that once the area at any longitudinal cross section was know, the volume was obtained by multiplication by the fuselage width. The cross sectional area was determined by dividing the side view into triangles and rectangles. This division could be done with a high degree of accuracy because the CAD points of the side view were known. Thus, for the fuselage volume we have:

$$Vf = 9.3 \times (A1 + A2 + A3 + \ldots + An)$$

where An = component area n.

The geometry of the wings and vertical stabilizers is slightly more complicated than that of the fuselage. For these shapes, an integral was used to find the volume. Both the wings and the stabilizers are diamond airfoils having five degree semi-vertex angles. Thus, from Figure 32, we see:

$$t(z) = c(z) \times \tan 5$$

where z = distance along span. Also from Figure 32, the cross sectional area is:

$$A(z) = [t(z) \times c(z)] / 2 = [c(z) \times c(z) \times \tan 5] / 2$$

We now only need the variation of chord with span, c(z). The wings are tapered from 10 feet at the root to 1 foot at the tip. Therefore: $c(z) = -3.7325 \times z + 10$

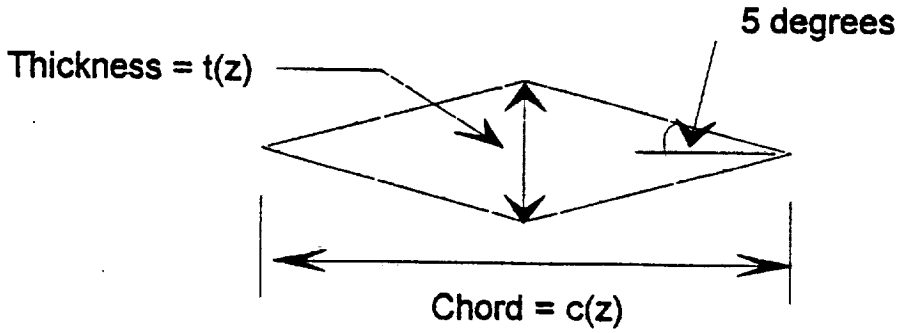

Figure 32: Diamond airfoil

Substitution of equation (4) into (3) and integration from z=0 to z=1 yields the wing volume. A similar analysis can be carried out for the vertical stabilizers, noting that the stabilizers are tapered from 6 feet to 0.5 feet and the integration should go from 0 to 1.5. The results of the volume analysis for the test vehicle are summarized in Table 12.

Fuselage Volume:	220 Cu. Ft.
Wing Volume	5 Cu. Ft.
V. Stabilizer Volume	3 Cu. Ft.
Total Vehicle Volume	228 Cu. Ft.

Table 12: Volume Results

Center of Gravity and Inboard Planfom:

As mentioned in the introduction, the most elegantly designed aircraft is rendered completely useless if sufficient room is not allocated for each system. For this reason it is important to generate a workable inboard planform. Also, the inboard planform is vital for the calculation of the CG. This section shall describe the internal layout and give the CG for the test vehicle as well as the vehicle plus booster system.

To generate the inboard planform, one must first size the systems to be included. For the test vehicle, these internal systems include; fuel, engines, payload, TPS, hydraulics, avionics/electronics (A/C systems), and the parachute or landing gear system. The payload volume is a design specification. The volume of the engines can be taken from GE data, while the fuel volume can be calculated from its mass using a liquid hydrogen density of 5.0 lbs/cu ft. The avionics/electronics volume can be calculated if we assume a "systems density" of 50 lbs/cu ft (Ref. 4). The volume required for the TPS, hydraulics, and electronics are disbursed throughout the plane in any available or needed area. For this reason, they do not fully appear in the planform shown (Figure 33). However, care was

taken to leave room for these systems. The volume required for each internal system is listed in Table 13.

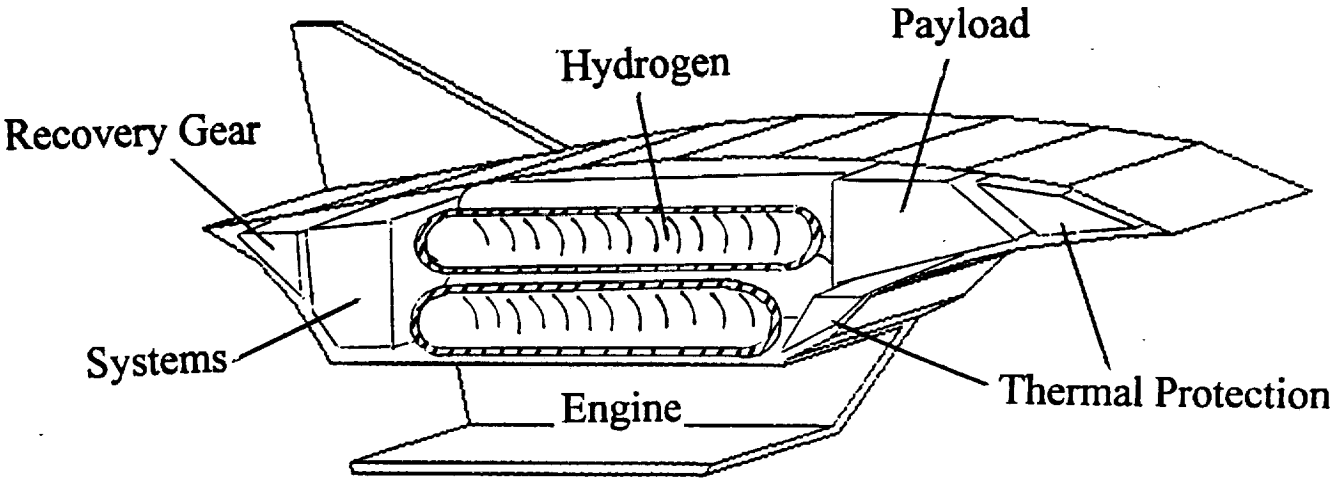

Figure 33: Inboard Planform

At this point, a discussion of the fuel tank system is appropriate. Given the fuel volume requirement, it was a bit of a challenge getting the fuel to fit. Originally, the idea

COMPONENT	Cubic Feet	% of fuselage
Avionics	21	12
Engines	43	22
Fuel	80	34
Payload	35	18
TPS	25	14

Table 13: Volume Required

of an integral fuel tank was explored, but this idea was abandoned after difficulty was encountered in finding room for it. The system shown includes four fuel tanks. This system does not carry with it the weight penalty of an integral tank, and it lends itself to fuel sequencing for the purpose of monitoring the CG travel during flight.

The center of gravity calculation was made using some simplifying assumptions. Because the placement of the TPS and hydraulics cannot yet be determined, these systems were modeled as point masses distributed throughout the body. Both were placed at the centroids of the wings and stabilizers, while the TPS was also placed at the leading edge of the fuselage. Also, the centroids of the empty fuselage, wings, and stabilizers were calculated assuming the bodies to be solids. The weight of these solids was determined by using an effective structural density multiplied by the body volume. The coordinate frame for the CG calculation is as shown on the inboard planform. Using the CG values, we obtain, for the test vehicle:

$Xc = 11.0$ ft $\qquad Yc = -.5$ ft $\qquad Zc = 0.0$ ft

As mentioned earlier, an attempt to use NASA's Hypersonic Aerospace Sizing Analysis (HASA) was made in order to develop initial estimates of test vehicle size and weight that could be used to verify results obtained from the methods decribed above. There were, however, two important inconsistencies between HASA and the initial design of the test vehicle. These two inconsistencies rendered HASA useless for the analysis of the test vehicle unless proper modifications were made. The PDWAP program was found much more effective and thorough.

8. Thermal Protection System

Because of the extreme temperatures expected during the flight of the aircraft the thermal protection system will be one of its most important systems. The cooling methods must be as light as possible in order to be incorporated into the airframe but still be highly efficient. It will be necessary to use both active and passive methods to keep the temperature within the operating tolerances of the aircraft.

Surface Temperature Determination

The first step in deciding which methods of thermal protection should be used is to determine the skin temperatures that the aircraft will experience during the flight. In order to find the local heat transfer coefficients, an algebraic approximation of more complex analysis methods was used. This approximation method shows good agreement with experimental results. In this method, the aircraft is broken into simple geometric shapes and each shape is analized a bit differently. The actual temperatures are found through an

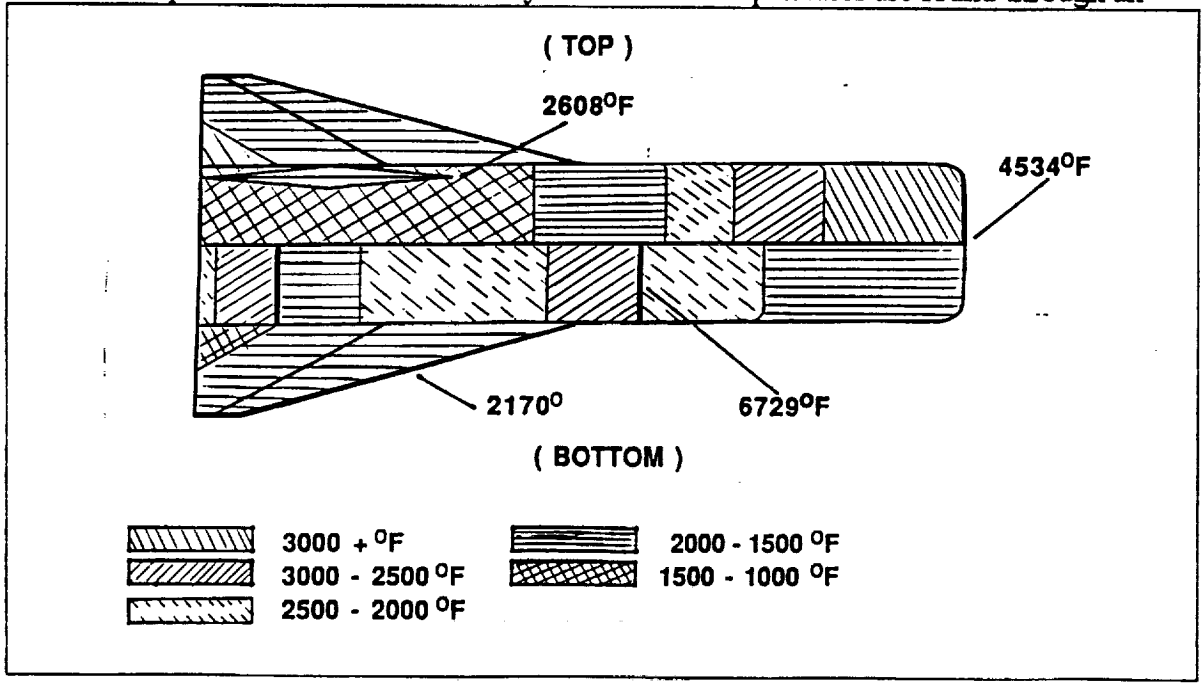

Figure 34: Thermal Map

iterative method using the heat transfer equations for both convecton and radiation. A temperature map of the entire surface of the aircraft was produced and is shown in Figure 34. These results were for a completely turbulent flow at zero angle of attack. The leading edge radii were based on aerodynamic data and came to be three quarters of an inch for the fuselage, a half inch for the wings and the vertical stabilizers, and one inch for the leading edge of the engine inlet.

Cooling Systems - Active and Passive

The passive cooling abilities of the aircraft will be required to be effective enough so that the active systems can be concentrated in a limited number of areas. In order to achieve this, advanced materials such as metal-metal composites, carbon-carbon composites, and others were examined and compared. Figures 35 and 36 show two of the comparisons that were made to determine which of the materials were feasible. The conclusion that can be drawn from the the figures is that only carbon-carbon composites have the ability to withstand the maximum temperatures that will be encountered by this aircraft. Also, the skin of the aircraft needs to be as

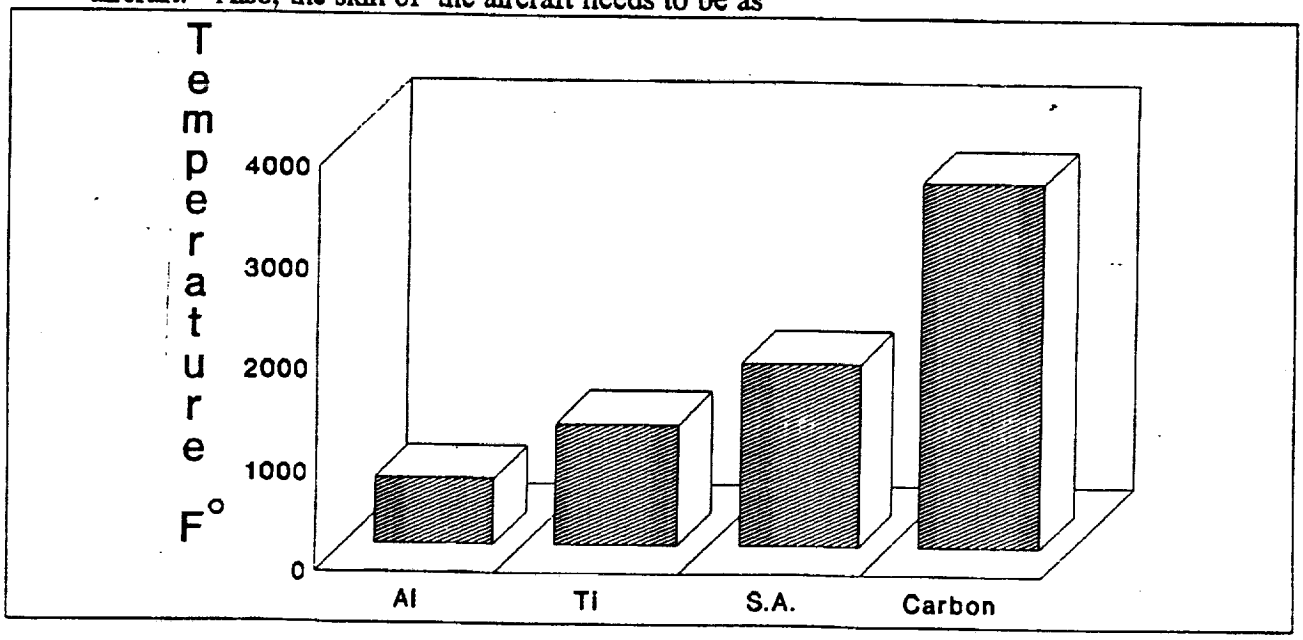

Figure 35: Comparison of Materials by Maximum Service Temperature

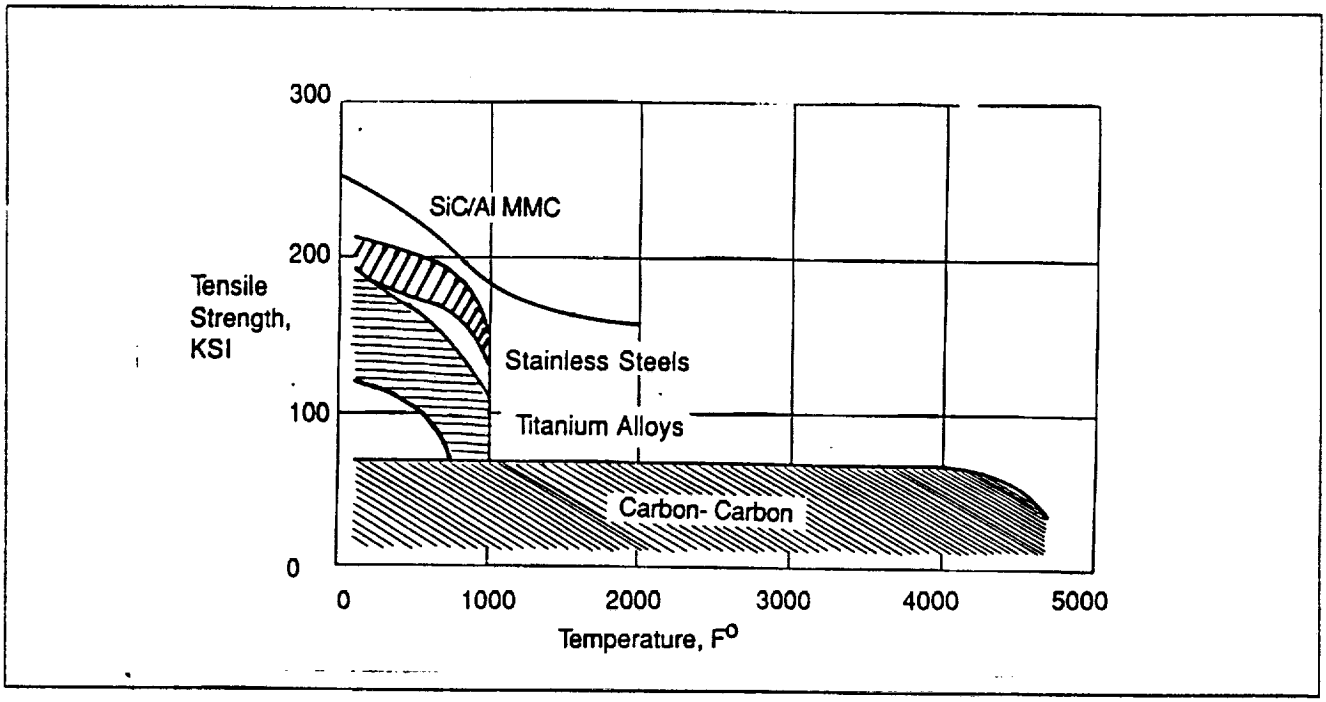

Figure 36: Comparison of Possible Skin Materials

radiative as possible in order to passively rid the aircraft of heat and again carbon-carbon with an emissivity of 0.8 seemed to be the best choice. Using this reasoning, carbon-carbon was chosen as the skin material for the entire aircraft. It was used for the entire plane because if multiple materials were used the interfaces between the materials would have to be dealt with and making the entire skin out of one material would avoid this problem. An important consideration for this data is that it does not take into account a reactive environment. Carbon-carbon cannot be used in a reactive environment because it quickly breaks down. Therefore, a protective coating must be applied to the outer surface. Two different coatings were chosen to protect the skin at two different temperature ranges. A boric oxide coating was used for areas that experienced temperatures less than 2500 F° and a hafnium boride and silicon carbide mixture was used for areas that experienced temperatures above 2500 F°. The second coating has the advantage that if its thickness is

increased the coated area can experience higher temperatures or the same temperatures for longer periods of time.

Insulating materials would also have to be utilized in order to protect the more sensitve internal systems and to keep the fuel system at the very low temperatures required. This portion of the thermal protection system was not researched extesively for this report since the exact temperatures that the internal systems can withstand must be known.

An active thermal protection system would definitely be needed at the leading edges where the maximum temperatures occurred. The methods of transpiration cooling, film cooling, and spray cooling were unlikely choices for this aircraft because each of these required large amounts of coolant which was not reused. Direct and indirect convective cooling were more likely choices because they both used the fuel which was onboard the aircraft as a heat sink (Figure 37 and 38).

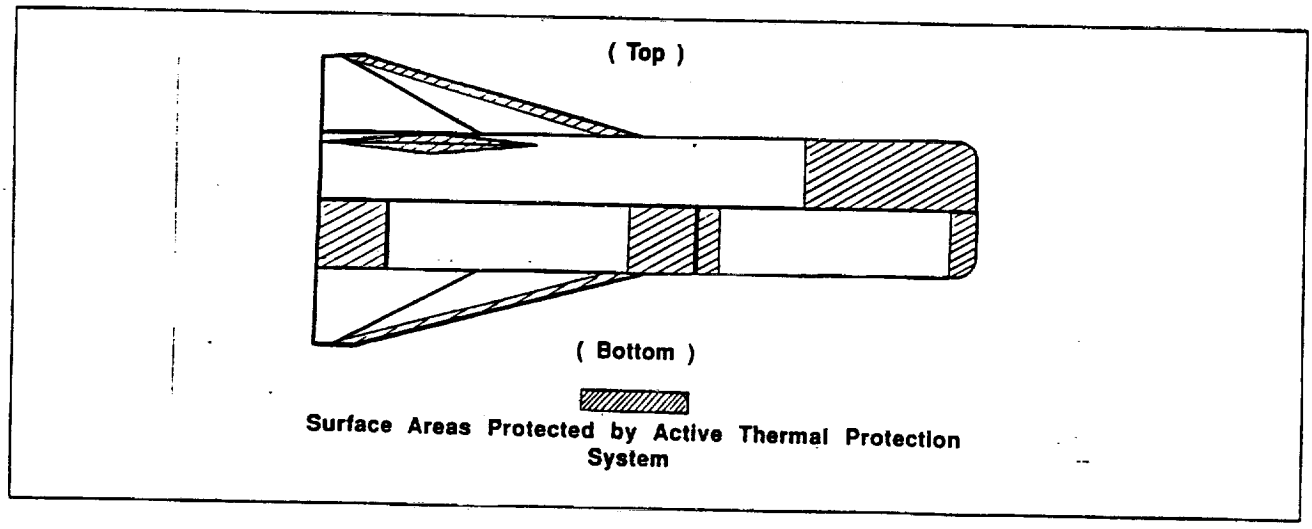

Figure 37. Indirect Active Cooling System

Although the direct cooling was a simpler concept, its drawbacks included the inherent dangers of pumping hydrogen throughout the airframe and the need for the cooling system and the propulsion system to have the same flow rate needs. The indirect method is more flexible because it uses a seperate coolant to circulate between the high temperature regions and the heat sink, but this flexibility is countered by an increase in weight due to the

addition of the coolant and a heat exchanger. The heat exchanger is needed to transfer the heat from the coolant to the fuel. Another complication of this method is that an appropriate coolant must be chosen. The coolant must have suitable heat storage and transfer capabilities, and it must be compatible with the aircraft components. Since the aircraft will not be igniting its engines until it has already achieved the cruise conditions and therefore will be traveling at constant conditions and since we wanted the plane to be as small and light as possible, the direct method of cooling was chosen for the aircraft. The placement of the active system is shown in Figure 39. This active system also protected the engine which must operate at extreme temperatures.

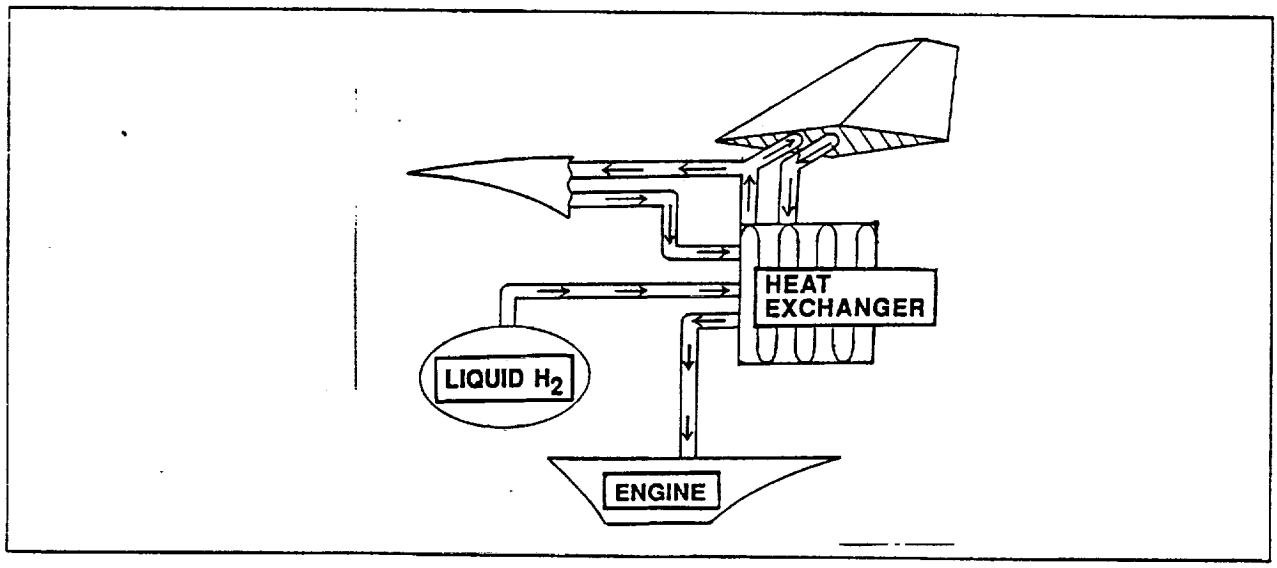

Figure 38. Direct Cooling System

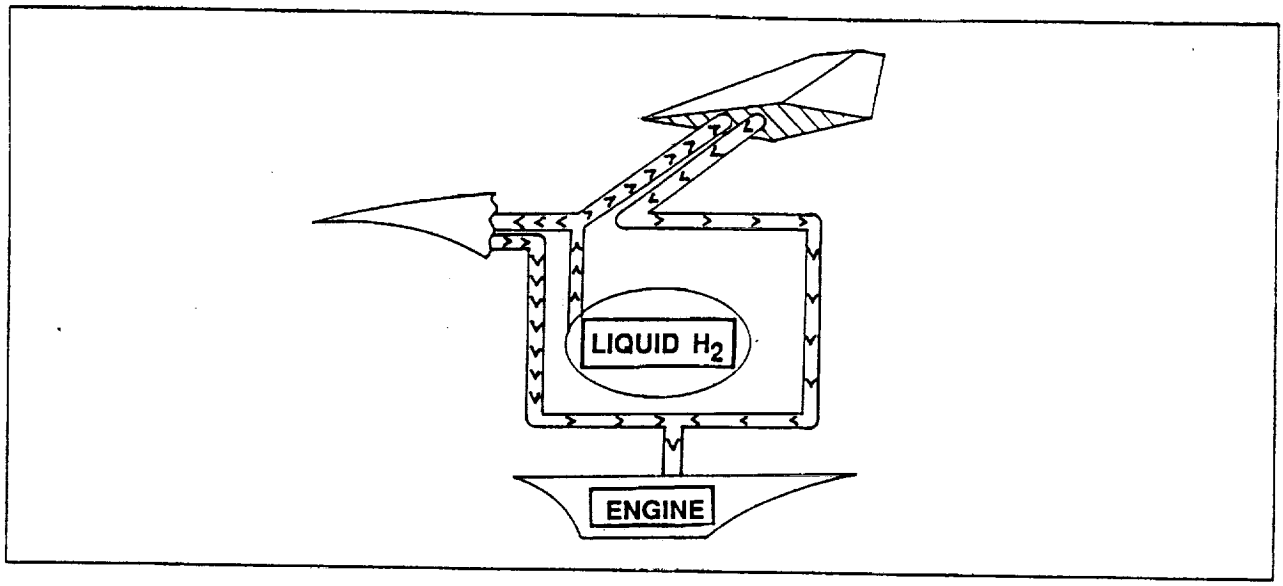

Figure 39. Active Thermal Protection System Layout

Conclusion for Thermal Protection Systems

The preceeding paragraphs have outlined the work and line of thought that has gone into the thermal protection system. With respect to temperature determination, a more acturate analysis using both laminar and turbulent flows should be done. Also, the rocket boosters and sheath must be analyzed so that it can be determined if they will need a thermal protection system. Finally, the skin temperatures throughout the flight of the aircraft must be found so that the exact thermal protection needs can be determined at any point during the flight. Once the rest of this is done, protection of the internal systems can also be looked into.

9. Cost Analysis

To analyze the cost of our vehicle, the empirically derived method from the design book was incorporated. The analysis represents three test vehicles flying a total of ten missions. Costs were originally calculated to 1986 dollars and then converted to 1993 dollars using a constant inflation rate of 3.5%.

The empirical equations use the structural weight, cruise speed, and aircraft quantity as the main determinants of cost. Because of our high cruise speed, every team adjusted the exponent on the speed using a factor average of 0.7. Refinement of the equations could help create much more accurate numbers. Projected inflation will increase cost, as would inclusion of high-tech materials costs. With this in mind, Table 14 provides the cost breakdown of the three vehicles. As this shows, the total cost of the project in 1993 dollars is $361,610,000. This translates to $448,000,000 in the year 2000.

Table 14: Cost Breakdown

Engineering Hours	**$ 78,780,000**
Development Support	**$ 17,350,000**
Flight Test Operations	**$ 9,580,000**
Tooling	**$ 41,490,000**
Manufacturing Labor	**$ 89,080,000**
Quality Control	**$ 11,580,000**
Engines	**$ 49,490,000**
Avionics	**$ 14,310,000**
Materials and Facilities	**$ 49,950,000**
TOTAL	**$361,610,000**

10. Conclusion

This report presents one possible design for an unmanned hypersonic vehicle that cruises at Mach 12 for one minute. All major areas of development are presented. We believe that our design is guinely realistic, but could use further optimization. The following conclusions can be drawn:

- The lifting body design is ideal for high hypersonic flight.
- Rocket boosters provide an excellent means of accelerating a hypersonic vehicle to test conditions.
- The small size of our vehicle is only limited by the comustion chamber length required of the scramjets and the payload burden.
- This design does not rely heavily on future technology and could be implemented in the near future.

Still, more research and optimization is needed. Future study is required, and recommendations would include the following:

- Model testing to confirm the subsonic characteristics.
- A comprehensive structural analysis.
- A further study of booster rockets and possible alternatives.
- Improving the descent trajectory
- An in-depth scramjet analysis
- Further analysis of the rear nozzle

Acknowledgements

The OSU II design team would like to thank the following persons for their assistance:

Dr. Gerald Gregorek

Dr. Rudolph Edse

Captain Carriero

Mr. Chris Snyder

Mr. Paul Barnhart

Duane Detwiler

Jeff Keip

Tim Higgins

Tom Ramsey

We would also like to thank The Ohio State Unversity Aeronautical and Astronautical Research Laboratory for the use of their Harris mainframe computer, and the staff of Wright Patterson Airfield for all their assistance.

References

Anderson, John D., Introduction to Flight, McGraw - Hill Book Co., New York, NY, 1989.

Anerson, John D., Modern Compressible Flow, McGraw - Hill Book Co., New York, NY, 1990.

Beck, Capt. William J. Jr., "TOPHAND" Profession Development Program, 1 Strategic Aerospace Division, Vandenberg AFB, CA

Beer, Ferdinand P. and Johnston, E. Russell Jr., Vector Mechanics for Engineers, McGraw - Hill, New York, NY, 1988.

Draper, Alfred C. and Buck, Melvin L., "Lifting Bodies - An Attractive Aerodynamic Configuration Choice for Hypervelocity Vehicles", Aeromechanics Division, Wright-Patterson AFB, Ohio, November 1986.

Glassman, Arthur J., "Airbreathing Propulsion for High-Speed Flight", NASA Lewis Research Center, Aeropropulsion Analysis Office, October 1992.

Mason, W. H. and Lee, Jaewoo, "On Optimal Supersonic/Hypervelocity Bodies", Virginia Polytechnic Institute and State University, 1990.

Nielson, Jack N., Missile Aerodynamics, McGraw - Hill, New York, NY, 1960.

Nelson, Robert C., Flight Stability and Automatic Control, McGraw - Hill, New York, NY, 1989.

Nicolai, Leland M., Fundamentals of Aircraft Design, METS Inc., San Jose, CA, 1975

Sin-I, Cheng, "Hypersonic Propulsion, Progress in Energy and Combustion Science", New York: Pergamon Press Inc., 1989.

Sutton, George P., Rocket Propulsion Elements, Fifth Edition, Wiley & Sons, 1986

"Research Vehicle Configurations for Hypervelocity Vehicle Technology", Boeing Defense and Space Group, Contract No. F33615-86-C-3004, Seattle, WA, 1991

General Electric Scramjet Engine Data, Cincinnati, OH

"Mach 6.5 Air Induction System Design for the Beta II Two-Stage-to-Orbit Booster Vehicle A.C. Midea", Sverdrup Technology, Inc., Sept. 1991, Baltimore, MA.

Transportation Research Circular, "Outlook for Commercial Supersonic and Hypersonic Transport Aircraft" No. 333, July 1988, Washington, D.C.